TH 1155

MIGMATIZATION AND VOLCANIC PETROGENESIS IN THE LA GRANDE GREENSTONE BELT, QUEBEC

Documents complémentaires

Additional Files

Licence

License

Énergie et Ressources naturelles
Québec

MIGMATIZATION AND VOLCANIC PETROGENESIS IN THE LA GRANDE GREENSTONE BELT, QUEBEC

BY

MIAN LIU

MCGILL UNIVERSITY

DECEMBER 1984

MIGMATIZATION AND VOLCANIC PETROGENESIS IN THE LA GRANDE GREENSTONE BELT, QUEBEC

By

Mian Liu

A thesis submitted to the Faculty of Graduate Studies and Research in partial fulfillment of the requirements for the degree of Master of Sciences

Department of Geological Sciences

McGill University

December 1984, Montreal

McGILL UNIVERSITY

FACULTY OF GRADUATE STUDIES AND RESEARCH

Date JANUARY 8, 1985

AUTHOR'S NAME MIAN LIU

DEPARTMENT GEOLOGICAL SCIENCES DEGREE SOUGHT: M.Sc

TITLE OF THESIS MIGMATIZATION AND VOLCANIC PETROGENESIS IN THE LA GRANDE GREENSTONE BELT, QUEBEC

1. Authorization is hereby given to McGill University to make this thesis available to readers in a McGill University Library or other Library, either in its present form or in reproduction. The author reserves other publication rights, and neither the thesis nor extensive extracts from it may be printed or otherwise be reproduced without the author's written permission.

2. The authorization is to have effect on the date given above unless the Executive Committee of Council shall have voted to defer the date on which it is to have effect. If so, the def rred date is:

Mian Liu

Signature of Author

Permanent Address:

4 Building 40, N-District

4th Oil Cop Shenze

Hebei, PRC

Signature of Dean required if date is inserted in paragraph 2.

(Français au verso)

To My Parents

For Their Love

ABSTRACT

This thesis concerns the tectonic evolution of the La Grande greenstone belt and the neighbouring gneissic-granitic terrane in the James Bay area of central Quebec. Two sequences of basalt and an overlying komatiitic sequence have been recognized in the study area. The geochemical variation of the basalts is compatible with a crystal-fractionation controlled magma evolution. Crystallization calculations suggest that the evolution of the basaltic magmas may have been somewhere between fractional crystallization and equilibrium crystallization, with most olivine and some pyroxene crystals removed while most plagioclase and some pyroxene crystals remained in the magma. The observed abnormal behavior of Rb and K is intepreted to result from contamination by continental crust when the magmas passed through it.

Despite the intimate spatial relationship of the komatiites to the basalts, and their similar trace element ratios, the basalts cannot be derived directly from the komatiites by fractionation. They may, however, have been derived from the same mantle diapir at different depths during rifting. A comparison with the geochemistry of basalts in other sections of the La Grande greenstone belt leads to a westward-propagating rifting

model for the tectonic evolution of the whole belt.

Migmatization is widespread in the gneissic-granitic terrane. Mass-balance calculations show that the low grade migmatite may have formed in an approximately closed system, controlled dominantly by partial melting. However, the generation of diatexite and anatectic granite involved significant mass transfer, particularly the gain of K and loss of Mg, Ca, Al and Na by the system. This may be due to the introduction of a metamorphic fluid, which may have been produced during crustal thickening following the rifting event.

RESUME

Cette thèse a pour sujet l'évolution tectonique de la ceinture de roches vertes de La Grande et des blocs gneisso-granitiques voisins, dans la région de la Baie de James, au centre du Québec. Deux séries basaltiques surmontées d'une série komatiitique ont été identifiées dans la region d'étude. La variation geóchimique des basaltes est compatible avec une évolution magmatique gouvernée par une cristallisation fractionnée. Les calculs de cristallisation suggèrent que l'évolution des magmas basaltiques représente un régime intermédiaire entre la cristallisation fractionnée et la cristallisation à l'équilibre, où la majeure partie de l'olivine et certains cristaux de pyroxenes ont été extraits du magma alors que la majeure partie du plagioclase et certains pyroxènes restaient dans le magma. Le comportement anormal du Rb et du K est interprété comme un effet de contamination crustale lors de l'intrusion de la croûte continentale par les magmas.

Malgré les relations spatiales intimes des komatiites et des basalts et la similarite de leurs rapports d'elements en trace, les basaltes ne peuvent avoir été derivés directement des komatiites par fractionnement. Ils pourraient toutefois provenir d'un diapir mantélique commun mais à des profondeurs différentes.

Une comparaison avec la géochimie de basaltes d'autres régions de la ceinture de roches vertes de La Grande suggère un modèle d'évolution tectonique de rift se propageant vers l'ouest pour la ceinture entière.

La migmatisation est fréquente dans le bloc gneisso-granique. Des calculs de bilan massique montrent que la migmatite de degré faible pourrait avoir été formée en système pratiquement clos, contrôlé principalement par fusion partielle. Par contre, la génération de diatexite et de granites anatectiques a dû impliquer un transfert de masse significatif, et en particulier le gain de K et des pertes en Mg, Ca, Al, Na par le système. Ceci pourrait être dû à l'introduction de fluides métamorphiques qui auraient été produits pendant l'épaississement crustal consécutif à l'événement du rift.

ACKNOWLEDGEMENTS

I would like to take this chance to express my sincere thanks to those who have generously offered me their assistance, help and encouragement during this work. My sincere thanks are due to Dr.A.Hynes, my thesis supervisor. He helped me in many aspects of the work. Many ideas in the thesis originated from stimulating discussions with him. I appreciate especially the effort he expended in improving the manuscript of this thesis. I am very grateful to Drs. D.Francis and R.Martin for their critical comments on parts of the manuscript. Dr. D.Francis kindly provided the computer program for crystallization calculations. I acknowledge gratefully the field assistance of S.Baillie, who suffered the discomfort from bugs and bears with remarkable courage. I also wish to thank T.Skulski and B.Rivard for their considerate help throughout the work; and T.Ahmedali and M.Mackinnon for their enthusiastic assistance in the analytic work.

I have been lucky to share an office with R.Stevenson and R.Leonard, their optimisim has maintained the office a place full of good cheer and companionship. My most sincere thanks are due to the Thomas', their love, hospitality and apple pies made my two-year stay in Canada much easier.

Financial support from the Clifford Wong fellowship (McGill

University), the Ministere de l'Energie (Quebec) and Reinhardt Summer Awards (the Department of Geological Sciences at McGill University) are gratefully acknowledged. The field and research work were supported by grants from NSERC (Canada), Ministere l'Education du Quebec and the Centre for Northern Studies at McGill University to Dr. A.Hynes.

TABLE OF CONTENTS

Page

List of figures

List of plates

List of tables

1. INTRODUCTION ---------- 1

1.1 Archaean greenstone belt ---------- 1

1.2 Location, previous work and geological setting ---- 5

1.3 Aim of the study ---------- 7

2. PETROGENESIS AND TECTONIC EVOLUTION OF THE GREENSTONE BELT ---------- 8

2.1 Feild features and petrography ---------- 9

2.2 Geochemistry ---------- 11

2.3 Evolution of the basaltic magma ---------- 18

2.4 Petrogenesis of the komatiite ---------- 23

2.5 Relationship of the komatiite to the basalt ------ 23

2.6 Tectonic evolution ---------- 27

2.7 Conclusions ---------- 31

3. MIGMATIZATION IN THE GNEISSIC-GRANITIC TERRANE ----- 39

3.1 General geology and petrography ---------- 30

3.2 Controls of migmatization ---------- 43

3.3 Mass transfer in migmatization ---------- 47

3.4 Discussion and conclusions ---------- 55

4. SUMMARY AND CONCLUSIONS ---------- 61

Contributions to the knowledge ---------- 65

Suggestions for future work ---------- 67

REFERENCES ---------- 68

APPENDIX I. ANALYTICAL PROCEDURES ---------- 76

APPENDIX II. BULK COMPOSITIONS OF THE ROCKS ------- 78

APPENDIX III. GEOTHERMOMETRY ---------- 85

APPENDIX IV. MINERAL COMPOSITIONS ---------- 87

APPENDIX V. GEOLOGICAL MAP OF THE STUDY AREA

LIST OF FIGURES

Figure	Page
1.1 Location of the La Grande greenstone belt	4
2.1 Stratigraphy and major structure of the greenstone belt in the study area	10
2.2 Variation of Rb, K, Zr and MgO in the study area	13
2.3 TiO2 vs. MgO in the study area	13
2.4 Mg vs. Fe for the La Grande greenstone belt	15
2.5 Al vs. Si in the study area	15
2.6 Y vs. Zr and Y vs. Ti in the study area	17
2.7 Cr, Ni, Rb and K vs. Zr in the study area	19
2.8 Relationship of the komatiite to the basalt in Al-Si space	25
2.9 Isomolar pseudo - liquidus phase diagram for the La Grande greenstone belt	28
2.10 C. (CaO + Na2O + K2O) vs. MgO for the La Grande greenstone belt	28
2.11 Rifting-propagation model for the evolution of the La Grande greenstone belt	29
3.1 Average temperature of the migmatization as a function of distance away from the biotite gneiss along the outcrop	44
3.2 Normative compositions of the migmatites in the Qz-Ab-Or ternary field	44
3.3 Mass transfer in the formation of the anatectic granite with restite as pure biotite	51
3.4 Mass transfer in formation of the anatectic granite with a modelled restite, (Bio50 P150)	53

LIST OF TABLES

Table	Page
2.1 Geochemistry of the volcanic rocks	33
2.2 Crystallization calculations using major element	34
2.3 Crystallization calculations using trace element	34
2.4 Crystallization calculations for the relationship between the komatiite and the basalt	34
3.1 Bulk compositions of the migmatites	57
3.2 Test of a closed-system of migmatization	57
3.3 Mass-balance calculations	58

LIST OF PLATES

Plate Page

3.1 migmatite ---------- 41

A. Metatexite

B. Diatexite

C. Anatectic granite

Chapter 1

INTRODUCTION

1.1 Archaean greenstone belts

Archaean greenstone belts are the oldest volcano-sedimentary successions on earth. They may bear the key to the understanding of the early crustal evolution of the Earth. These belts vary in size from a few to hundreds of kilometres wide, and are commonly linear and surrounded by gneissic-granitic terranes. Typical greenstone belts are synclinally deformed, with a threefold division of stratigraphy: an ultramafic-mafic lower part, a calk-alkaline middle part and a sedimentary cover (Anhaeusser et al. 1969; Anhaeusser 1971; Glikson 1976), although this regular succession is by no means true of all of them. Most of them are metamorphosed to greenschist facies.

The ultramafic-mafic volcanic sequences form the major part of most greenstone belts. The mafic volcanic rocks are generally geochemically similar to mid-ocean-ridge basalts. This led to early ensimatic models for greenstone belts. (e.g. Viljoen and Viljoen 1970, Glikson 1972; Anhaeusser 1973). However, greenstone belts in which the volcanic rocks rest directly on granitic basement have been found in recent years (e.g. Bickle et al. 1975; Ramakrishnan et al. 1976; Henderson and Easton 1977), indicating an at least partly intracontinental (ensialic)

evolution. The recognition of plate tectonics stimulated many analogous models for the evolution of greenstone belts. One of the most popular ideas is that greenstone belts have originated in a marginal-basin environment (Burke et al. 1976; Tarney et al. 1976). Tarney et al.(1976) argued that the high contents of Cr, Ni and also large-ion-lithophile elements (K, Rb, Ba) of typical greenstone-belt basalts are similar to those of marginal basin basalts. They provided a comparable modern example for the marginal basin model, the Rocas Verdes complex in southern Chile. There, mafic volcanic sequences were formed through back-arc spreading and then deformed with subsequent convergence of the plates. The geochemical and stratigraphic characteristics of the complex are similar to those of greenstone belts. Windley (1977) developed this model, interpreting the high-grade gneissic complexes as the main arc batholiths, and proposed a modified marginal-basin model for greenstone belts and the surrounding gneissic-granitic terranes. This model is generally consistent with the geochemistry and stratigraphy of greenstone belts and their field relationships to the neighbouring gneissic terranes. Another popular model is the formation of greenstone belts following continental rifting (e.g. Kroner 1981; Lambert 1981). This model also accounts well for the geochemistry and stratigraphy observed in some greenstone belts.

One of the best studied greenstone belts is the Abitibi greenstone belt in the Superior Province of the Canadian shield. It is 700 km long and 200 km wide and trends easterly, and is

composed of several elliptical volcanic complexes. Its tectonic evolution is still controversial. One school of thought suggests that it formed in a rifting environment (e.g. Goodwin 1977; 1982). Recent isotopic work of Gariepy et al.(1984) indicates a sialic basement closely associated with the development of the Abitibi volcanic rocks. This seems to favour the continental-rift theory. On the other hand, Dimroth et al. (1982; 1983) proposed an island arc - fore-arc basin setting for the belt, mainly based on structural patterns.

Thus the mechanism of the evolution of greenstone belts is controversial. It seems that greenstone belts may have formed in various tectonic environments. Studies of geochemical evolution of greenstone belts, although they cannot be used in isolation, may provide some of the most powerful constraints on their origin.

In contrast to the great amount of work that has been devoted to greenstone belts, little has been done in the neighbouring gneissic-granitic terranes, which are however of great importance for a comprehensive understanding of the crustal evolution. In this thesis a preliminary study of the La Grande River greenstone belt and the surrounding gneissic-granitic terrane is presented, with the aim of constraining the origin of the greenstone belt and the neighbouring gneissic-granitic terrane.


80°
56°
76°
72°
La Grande River
JAMES
BAY
Eastmain
Bolt
52°
Abitibi Bolt
Kilometre
100
0
100

Fig. 1.1

1.2 Location, previous work and geological setting

The La Grande greenstone belt in the James Bay area of central Quebec is about 600 km north of the Abitibi greenstone belt. It is 350 kilometre long. Like the Abitibi belt, it trends easterly, and lies to the south of the La Grande River (Fig. 1.1). With the surrounding gneissic-granitic terrane, it comprises part of the Archaean Superior province, which has U-Pb zircon ages between 2700 and 2550 Ma. (Anderson and Gast 1965; Tilton and Steiger 1969; Hart and Davis 1969). No dates are avaible for the La Grande greenstone belt itself.

Early mapping of this region by the Geological Survey of Canada on a reconnaissance scale of 1:1,000,000 was reported by Eade (1966). In 1974, Mills prepared a doctoral thesis based on mapping of Sakami Lake area, in the eastern part of the belt (Mills 1974). Sharma (1975) and Larose (1975) mapped part of this region on scales of 1:125,000 and 1:50,000, respectively. More recently, St.Seymour mapped the Lac Guyer area and discussed

---

Fig.1.1. The location of the La Grande greenstone belt. The black square with the arrow is the area mapped in this work. Numbered squares are the areas studied by other authors: 1 - Lac Guyer area (St. Seymour 1982; St. Seymour et al. 1983); 2 - LG3 area (Skulski et al. 1984); 3 - LG2 area (Rivard and Francis 1984).

the magma evolution in a doctoral thesis submitted to McGill University (St.Seymour 1982). In the summer of 1983, detailed mapping was carried out by Rivard in LG-2 area, Skulski in LG-3 area and the author, in an area between LG-3 and LG-4 hydropower stations (Fig. 1.1).

The study area of this thesis is located about 80 kilometres west of LG-4 (Latitude 53° 30', longitude 75° 15'). A road from Matagami (500Km southwest of the study area) connecting LG-2, LG-3 and LG-4 makes access to this area very easy. Vegetation cover is poor and the exposure of rocks is over 50 percent. This area is glaciated with numerous lakes and swamps. A 2000 metre thick volcanic succession of the La Grande greenstone belt is well preserved here and bounded on both sides by the gneissic-granitic terrane (Appendix-V). It is composed of a lower unit of massive basalts interbedded with mafic and felsic tuff, a middle unit dominated by strongly flattened pillowed basalts, and an upper komatiitic sequence. The rocks are metamorphosed to amphibolite facies and deformed into a south-vergent, overturned syncline.

The major types of rock in the neighbouring gneissic-granitic terrane are biotite paragneiss, granite, granodiorite, migmatite and pegmatite. They are irregularly distributed and commonly gradational into one another. At the northern margin of the greenstone belt, granodiorite intrudes the volcanic succession. The relationship of the greenstone belt to the

gneissic-granitic terrane at its southern margin is not apparent, due to the intensity of deformation. Descriptions of the field features and petrography of the rocks in the greenstone belt and the gneissic-granitic terrane are given in the following chapters.

1.3 Aim of the study

The generation of greenstone belts is a problem of broad scope, involving studies in many fields. This work is mainly focused on two aspects:

1) Magmatic evolution of the greenstone belt and the tectonic controls on this evolution;

2) Migmatization in the gneissic-granitic terrane, with emphasis on the controls on migmatite generation and the accompanying mass transfer.

These two problems are discussed separately in Chapters 2 and 3.

Chapter 2

PETROGENESIS AND TECTONIC EVOLUTION OF THE GREENSTONE BELT

The intimate spatial relationship of komatiites to basalts in Archean greenstone belts has led many authors to suggest genetic relationships between them (e.g. Arth et al. 1977; Arndt and Nesbitt, 1982; St.Seymour et al. 1983). However, in what way komatiites are related to basalts is still not clear. The evolution of basalts in greenstone belts is also poorly understood, partly because many Archaean basalts are extensively altered, making geochemical studies difficult. Another controversial problem associated with the development of greenstones is their tectonic environment, as discussed in the first chapter.

In this chapter the magmatic evolution of the La Grande greenstone belt and the tectonic controls on this evolution are discussed. The well exposed mafic volcanic succession with simple structure in the study area provides an opportunity to study the magmatic evolution of the greenstone belt. The systematic geochemical variations indicate that these rocks are not greatly affected by secondary processes. The relationship of komatiites to basalts and the evolution of the basaltic suite are examined using fractional crystallization and equilibrium crystallization calculations. The geochemical characteristics are compared with those of other sections of the greenstone belt and a model of rift-propagation is proposed for its tectonic

evolution.

2.1 Field features and petrography

A roughly 2 kilometre volcano-sedimentary succession of the La Grande greenstone belt is well exposed in the study area. The rocks are metamorphosed to amphibolite facies and deformed into a south-vergent, overturned syncline. On the northern limb of the syncline, two sequences of basalt (defined by geochemistry, see below) overlain by a komatiitic sequence may be recognized. The first basaltic sequence is much thicker than the second one. The southern limb is poorly exposed. There may be a reverse fault in the southern limb that foreshortens the thickness of the basalt (Fig. 2.1).

The lower basaltic sequence is composed of thick flows (generally 5 metres in thickness) of mafic lava at the base, interbedded with mafic and felsic tuffs. Its top part and the whole of the second sequence are dominated by strongly flattened pillow basalts. The basaltic rocks are commonly dark-green to black. The thick flows are fine to medium grained. The pillow basalts, commonly 30 centimetres long, are all fine grained, with clear chilled margins. Some plagioclase phenocrysts are observed in both thick flows and pillow basalts. The komatiites commonly show well developed polygonal joints. Their brown weathered surfaces with protruding olivine grains (0.5 cm in size) are very distinctive. Locally, spinifex textures are clearly preserved in the chilled margins.

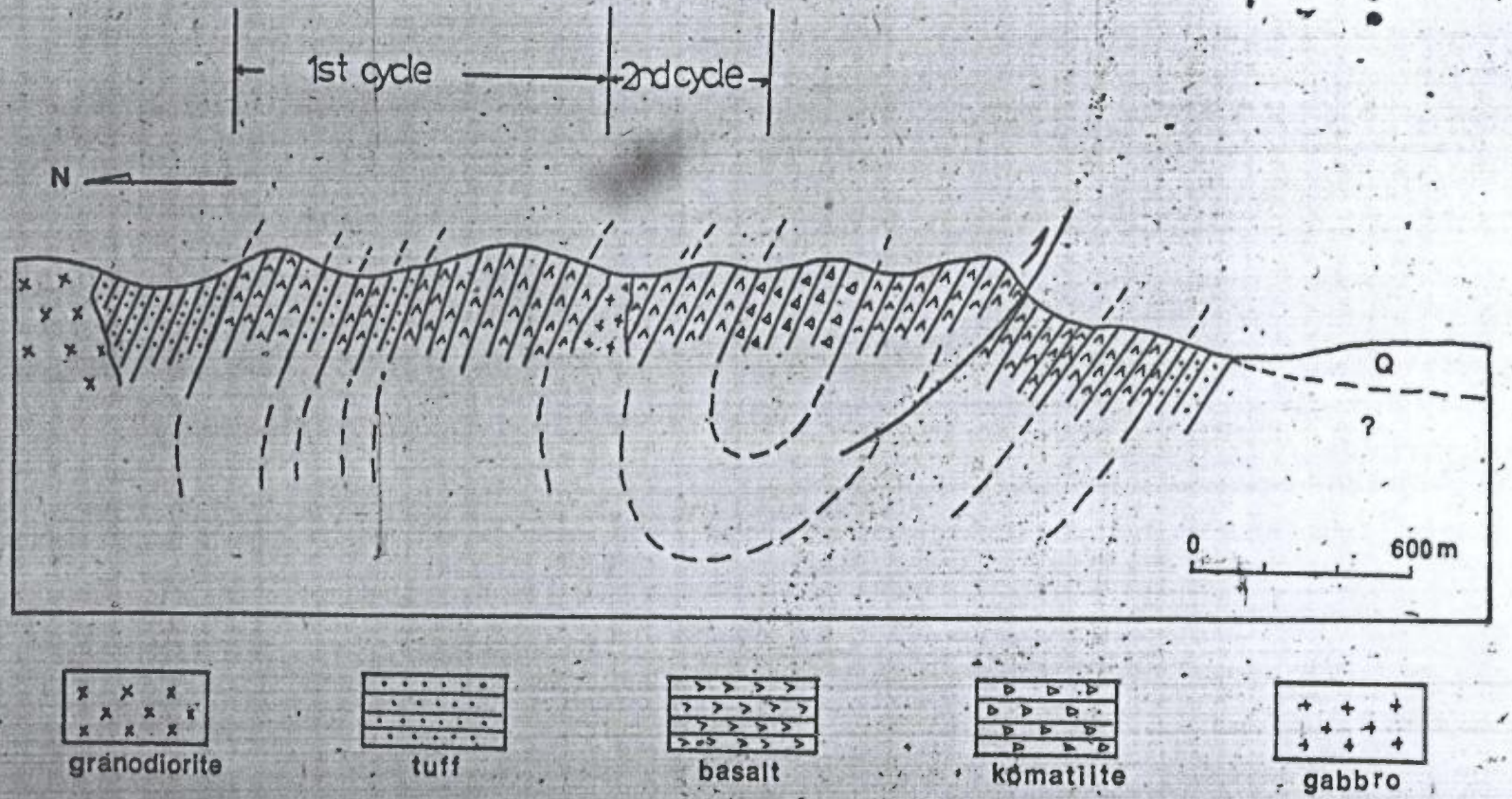
1st cycle
2nd cycle
N
Q
?
0
600m
granodiorite
tuff
basalt
komatiite
gabbro

Fig.2.1

The original mineralogy of these rocks has been almost completely replaced during metamorphism. The basalts are dominated by amphibole (over 70%), with fine-grained plagioclase (20-25%) and some chlorite. In the thick basaltic flows the amphiboles occur as randomly oriented phenocrysts and in clusters. They are commonly elongate and probably replaced original pyroxene and (or) olivine crystals. The pillow basalts commonly contain elongate amphibole phenocrysts (15-20%), embedded in a fine-grained matrix of amphibole and plagioclase.

The komatiites are commonly composed of large olivine grains, a fine-grained matrix of tremolite, serpentite and some chlorite. The olivines are probably of metamorphic origin (c.f. St.Seymour and Francis 1980). Some olivine spinifex textures are preserved by random and subparallel skeletal tremolite pseudomorphs.

2.2 Geochemistry

Basalt

Systematic variation of MgO and other elements in the basaltic suite indicates two sequences of eruption (Fig. 2.2). The high-Mg basalts (MgO = 9%) are olivine-normative, but some

---

Fig. 2.1. Stratigraphy and major structure of the greenstone belt in the study area.

low-Mg basalts (MgO = 5-6%) are quartz-normative. The general geochemical characteristics of these basalts are close to those of MORB, with slightly higher Si, Ti, Fe and lower Mg (Fig. 2.3, 2.4). In Mg-Fe space the basalt suite shows a clear Fe-enrichment trend, a feature of low-pressure crystal fractionation (Fig. 2.4). This is compatible with the negative correlation of Al and Si (Fig. 2.5).

The Zr/Y ratio (2.14) is almost identical to that of chondrites (2.2; Fig.2.6a). The Ti/Y ratio (364), however, is much higher than that of chondrites (256; Fig.2.6b). The Al2O3/TiO2 ratio (15.5) is also lower than that of chondrites (20.4; van Schmus and Hayes 1974). This may reflect derivation of the basalt from a mantle "undepleted" relative to that from which MORB are derived.

Komatiite

Mafic volcanic rocks with high MgO content (>35%) in this region occur generally in the centres of flows and are almost totally serpentinized. They were probably olivine cumulates (cf. St. Seymour 1982). The samples from chilled margins of thin flows (samples 039,040,052,071) with spinifex texture provide estimates of the liquid compositions of the komatiite flows. Their MgO contents vary from 22% to 31% (Tab. 2.1), and the average composition is close to that of the peridotitic komatiite in the Lac Guyer area (St.Seymour and Francis 1980). There is a

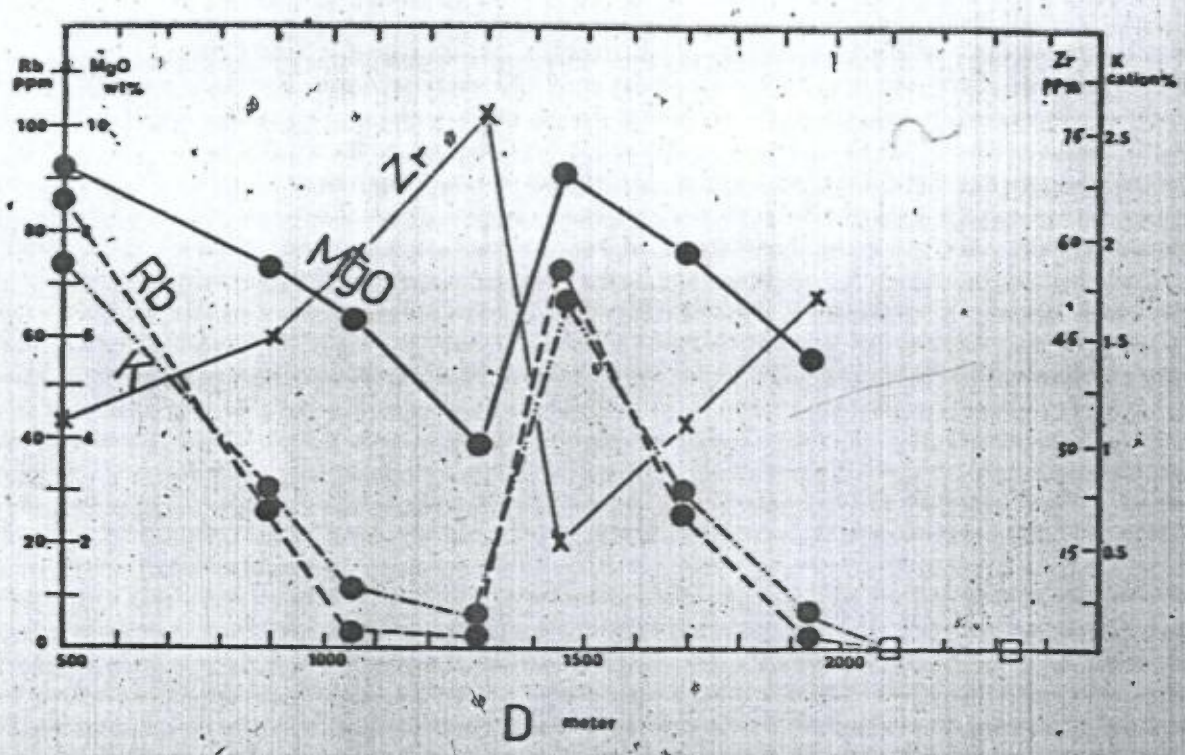
Rb ppm
MgO wt%
Zr ppm
K cation%
Zr
Mgo
Rb
K
100
80
60
40
20
0
10
8
6
4
2
75
60
45
30
15
2.5
2
1.5
1
0.5
500
1000
1500
2000
D meter

Fig. 2.2

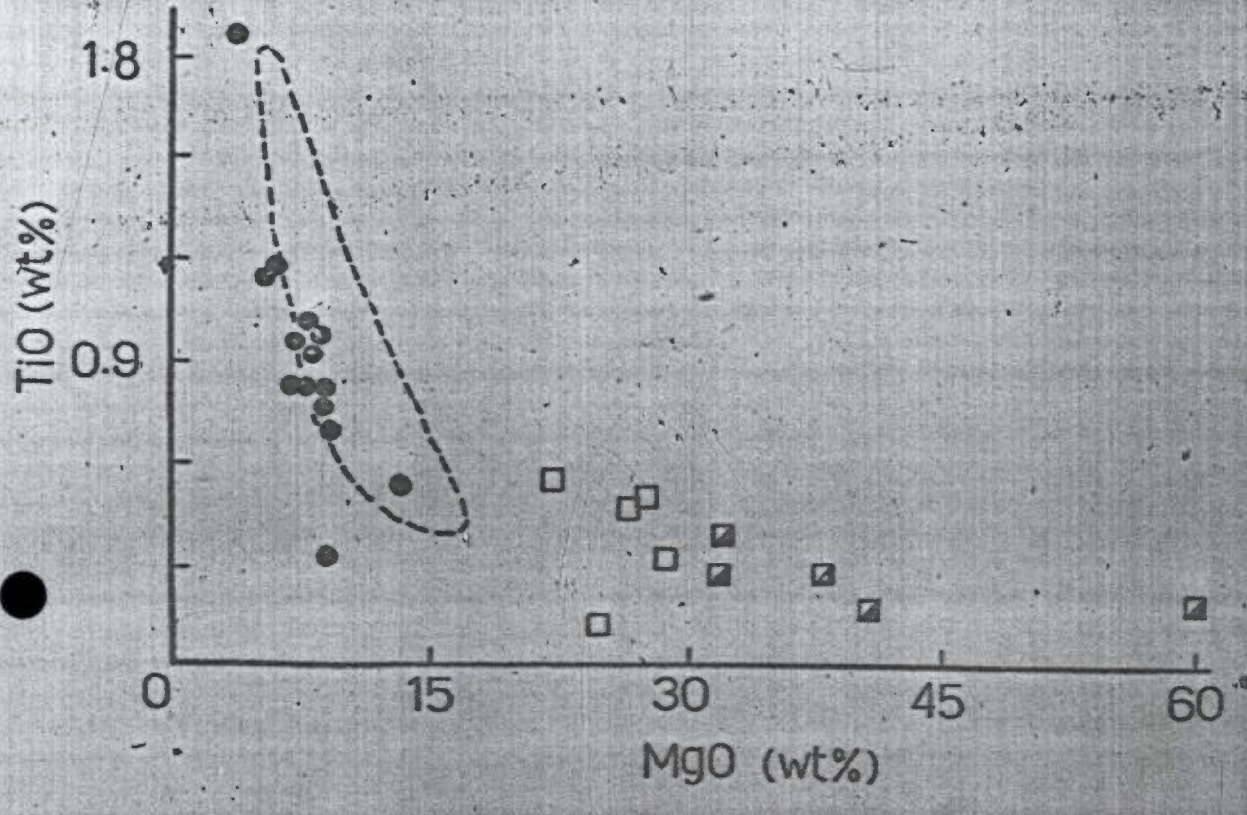
1.8
0.9
TiO (wt%)
0
15
30
45
60
MgO (wt%)

Fig. 2.2. Variations of Rb, K, Zr and MgO along a transect of the La Grande greenstone-belt in the study area. The horizontal axis represents the distance away from the northern margin of the greenstone-belt. Filled circles--basalts, open squares--komatiites. The samples of basalt are (form left to right) 83062, 83065, 83066, 83068, 83072, 83079.

Fig. 2.3. TiO2 vs. MgO in the study area. half filled squares are olivine-cumulates. Other symbols as in Fig. 2.2. MORB field is circled by the dashed line (Data of MORB used in the thesis are from Byerly and Wright (1978), Bryan (1979), Sun and Sharaskin (1979).

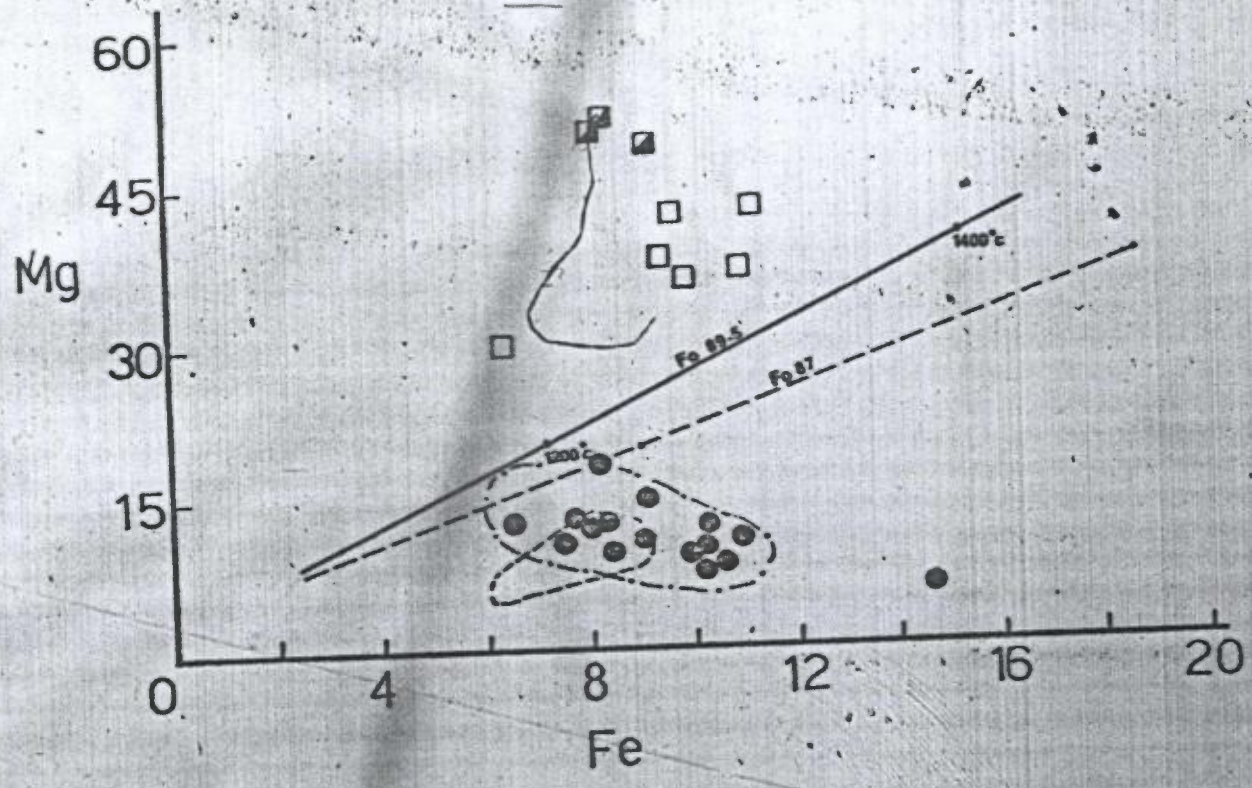
60
45
30
15
Mg
0
4
8
12
16
20
Fe
1400°c
1200°c
Fe 93.5
Fe 87

Fig. 2.4

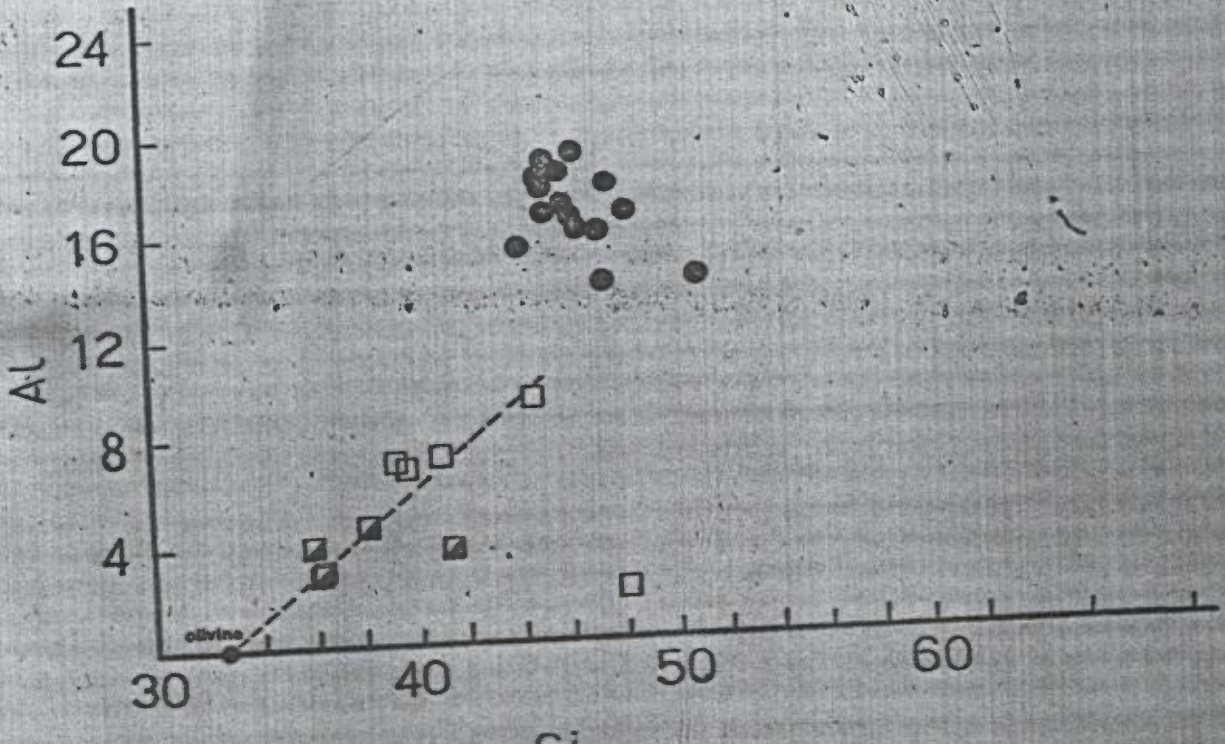
24
20
16
12
8
4
Al
30
40
50
60
Si
olivine

Fig. 2.5

Fig. 2.4. Mg vs. Fe (cation units) for the La Grande greenstone-belt. The two straight lines are the initial-melting line of the mantle obtained after the manner of Hanson & Langmuir (1978). Rocks below the initial-melting line are considered unable to coexist with the mantle. The solid line is for a pyrolite with an initial olivine composition of Fo 89.5. The dashed line is for the mantle composition proposed by Cater (1970), for which the initial olivine composition is Fo 87. The field circled by the dashed line encompasses data from the basalt suite in the LG 2 area, in the eastern part of this greenstone belt. The the field circled by the dot- and-dashed line is for MORB. Symbols as in Fig. 2.2, 2.3.

Fig. 2.5. Al vs. Si (cation units) in the study area. The komatiites and cumulates lie on an olivine-controlled line. The basalts show negative correlation of Al and Si. Symbols as in Fig. 2.2, 2.3.

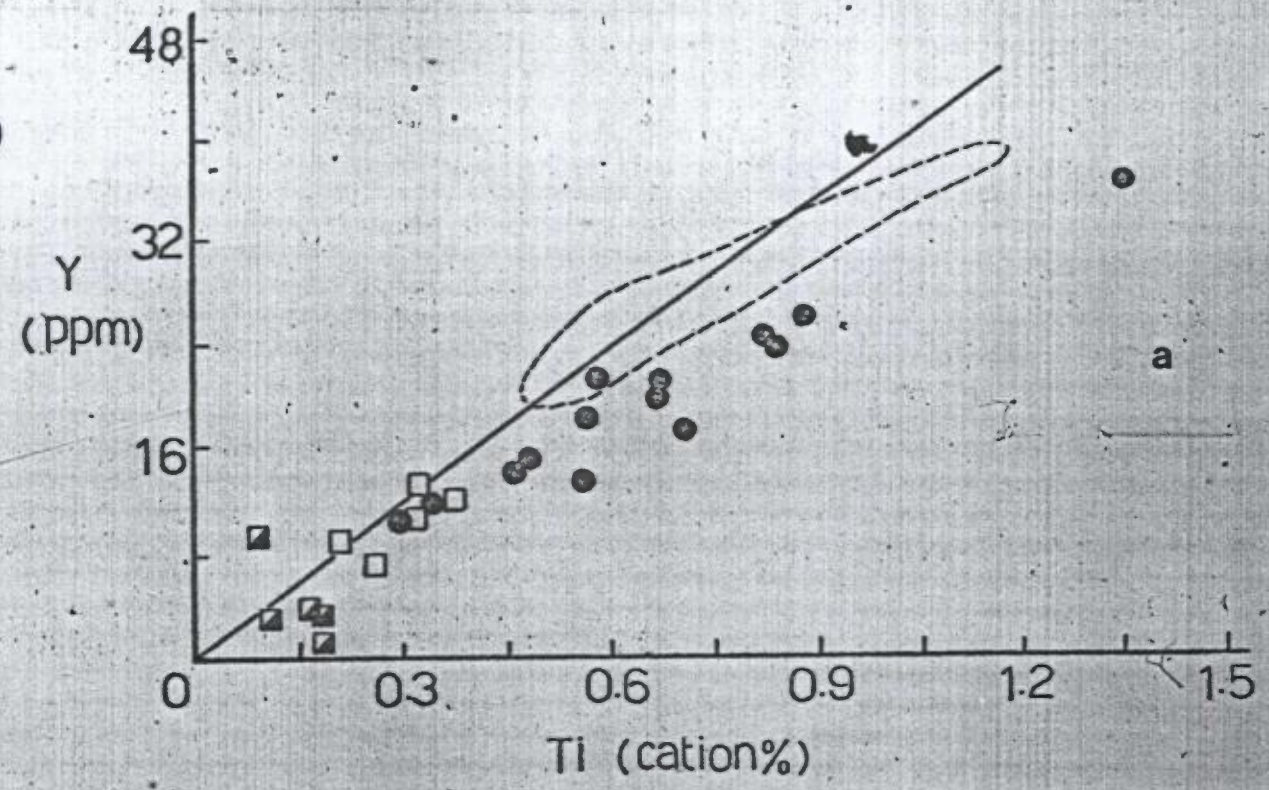
48
32
16
0
Y
(ppm)
0.3
0.6
0.9
1.2
1.5
Ti (cation%)
a

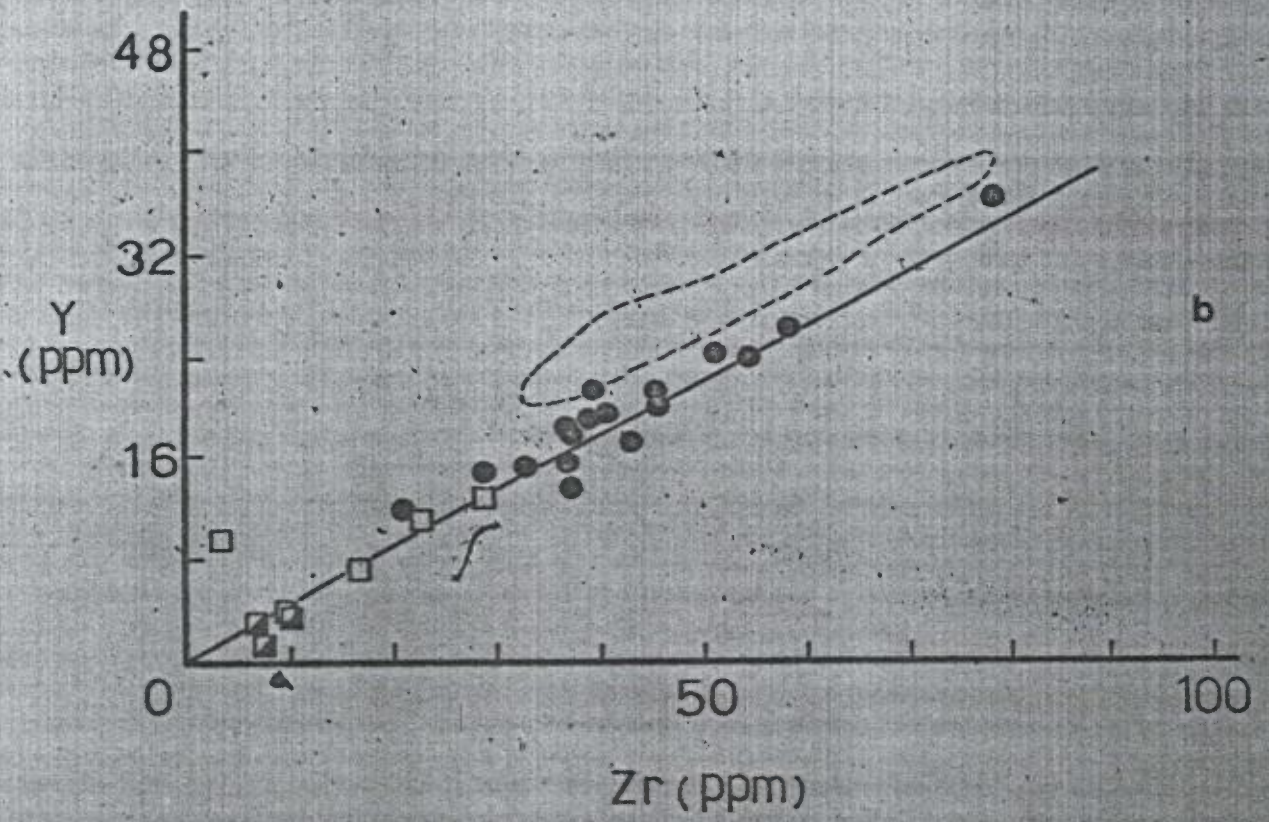
48
32
16
0
Y
(ppm)
50
100
Zr (ppm)
b

Fig 2.6

pronounced compositional gap between them and the basalts (Fig.2.3), which may be due to their different evolution histories (see St. Seymour et al. 1983). Their high Mg# (Mg/Mg+Fe* 0.8; Fe* is total iron), low TiO2 content(0.13-0.56%; see Fig.2.3) and an average CaO/Al2O3 ratio of 0.86 are characteristic of komatiites (Viljoen and Viljoen 1969; Nesbitt and Sun 1976). In Al-Si space they lie on an olivine-controlled line, which may reflect olivine dominated fractionation or olivine accumulation (Fig.2.5). The incompatible trace element ratios are similar to those of the basalts (Fig.2.6).

2.3 Evolution of the basaltic magma

The strong Fe-enrichment trend (Fig. 2.4), the upward decrease of MgO in each sequence of basaltic lava (Fig.2.2) and the rapid decrease of the highly compatible elements, Cr and Ni, as Zr increases (Fig.2.7) are compatible with a crystal-fractionation-controlled evolution of the basaltic suite. Equilibrium crystallization and fractional crystallization modelling was carried out to simulate the possible fractionation history. The results are presented in Table 2.2. 50 percent fractional crystallization of the high-Mg basalt with the mineral proportions of 26% olivine, 20% clinopyroxene, and 54% plagioclase produces a daughter magma whose composition is very

---

Fig. 2.6. Y vs. Zr and Y vs. Ti in the study area. The straight lines represent chondrite ratios of Zr/Y (2.2) and Ti/Y (256). Data from Wenke et al. (1974). Symbols as in Fig. 2.2, 2.3.

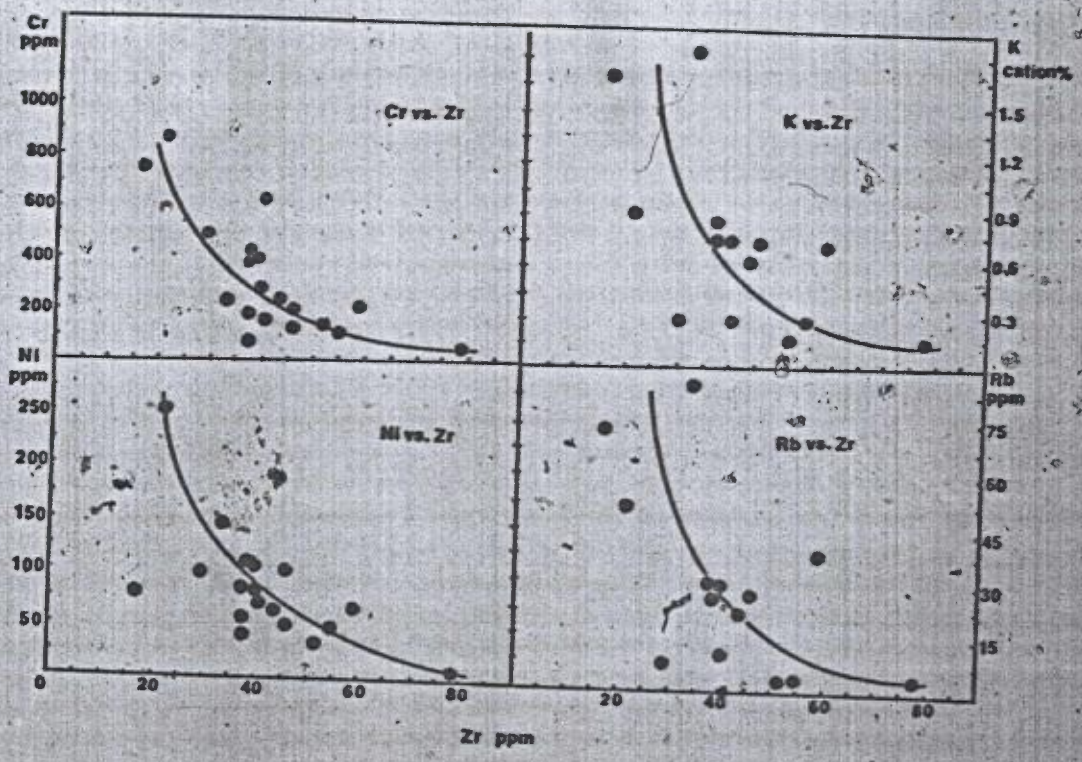
Cr ppm
1000
800
600
400
200
Cr vs. Zr
K cation%
1.5
1.2
0.9
0.6
0.3
K vs. Zr
Ni ppm
250
200
150
100
50
Ni vs. Zr
Rb ppm
75
60
45
30
15
Rb vs. Zr
0
20
40
60
80
Zr ppm

Fig. 2.7

close to that of the low-Mg basalt. The mineral proportions are slightly high in olivine compared with the 1 atm olivine-clinopyroxene-plagioclase cotectic (15,35,50 to 20,20,60; see Biggar 1983). This may reflect a slightly higher pressure of fractionation for the basalts in this greenstone belt (Increasing pressure shifts the cotectic towards olivine in the phase diagram (see Elthon 1984). On the other hand, high pressure would change the composition of fractionating plagioclase (Grove and Baker 1984). Because the mineral proportion we obtained is very close to that of 1 atm Ol-Cpx-Pl cotectic, and because the knowledge of high pressure fractionation is still poorly known, we shall not further discuss this problem here.) The equilibrium crystallization modelling, with mineral proportions of 28% olivine, 16% clinopyroxene and 56% plagioclase, results in a substantially Fe-poor daughter, but otherwise produces a very close fit (see Tab. 2.2. Possible reasons for the Fe-discrepancy, and a favoured crystallization model, are discussed below.)

Trace element concentrations were used to test the major-element-modelling. Their values in the high-Mg basalt, C'o, were calculated from those of the low-Mg basalt using the values of F given in Table 2.2, and D (bulk distribution coefficients) determined by the mineral proportions in the major element

---

Fig. 2.7. Compatible elements, Cr and Ni and mobile incompatible elements, K and Rb, versus Zr in the study area. Symbols as in Fig. 2.2, 2.3.

modelling (Tab.2.3) and the crystal/liquid distribution coefficients of elements (Pearce and Norry 1979; Cox and Pankhurst 1979). The modelled original element concentrations of Zr, Y and Ti are very similar to those observed in the high-Mg basalt. The low C'o for Cr may be due to a small amount of chromite involved in the fractionation, which is not accounted for in the modelling. The concentration of Ni in the high-Mg basalt (115 ppm) falls between the two modelled values, 161 ppm (for fractional crystallization) and 82 ppm (for equilibrium crystallization). Since Ni is partitioned dominantly into olivine during the fractionation (The mineral /liquid distribution coefficient of Ni is 10 for olivine), this requires that some of the olivine be removed from the magma during fractionation. The low Fe in the daughter magma derived from the equilibrium crystallization calculation also requires removal of olivine (Tab.2.2), which is the major Fe-carrier. Thus, the real fractionation process may have been somewhere between fractionation crystallization and equilibrium crystallization, with plagioclase and some pyroxene crystals staying in the magma while most olivine crystals were removed. Such a model is compatible with probable density contrasts between melts and crystals (c.f. Stolper and Walker 1980).

Rb and K, which usually behave like incompatible elements during fractionation, show trends similar to that of compatible elements during the evolution of the basalts (Fig.2.7). Although these elements are very mobile, the systematic variation of Rb

and K shown in Fig.2.2 indicates they are not greatly affected by secondary processes. In this figure we see their concentration decrease upwards in each basaltic sequence. One possible explanation for the high K and Rb basalts may be the mixing between a K-Rb-enriched and a K-Rb-poor end member. However, it would be difficult to explain why K and Rb show trends opposite to what they should be during fractionation in each basaltic sequence. On the other hand, if we assume the two end members are derived from the same source, it would be difficult to have an end member with much higher contents of K and Rb than the other end member while their other major element concentations are very similar. Another possible explanation, which is favoured in this work, is contamination by the continental crust when the magmas passed though it. Watson's (1982) experiments showed that when mafic magmas react with continental crust, K would increase greatly in the mafic magma while other major elements are hardly affected. Observations of selected contamination of K,Rb and other mobile lithophile elements have been reported by Dostal et al. (1983), Maury and Bizouard (1974) and Doe et al. (1969). The renewed high Rb and K at the onset of the second sequence (Fig.2.2) may mean that basalts of the second sequence erupted through another channel in continental crust after the activity of the first sequence had ceased. The komatiites, on the other hand, were not affected by this contamination, suggesting an oceanic crust was already formed by the time of their eruption. An alternative possibility would be that the komatiites erupted through the same channel as the second-sequence basalts.

2.4 Petrogenesis of the komatiite

Archean komatiites are generally believed to be products of large degrees of partial melting of the upper mantle (Nesbitt and Sun 1976; Arth et al. 1977; Nisbet 1982). St. Seymour et al. (1983) documented a komatiitic suite ranging in composition from perioditic komatiite to pyroxenitic komatiite in the Lac Guyer area, east of the study area. They suggested that it represented a series of magmas produced by progressively increasing degrees of partial melting of a garnet lherzolite mantle. No pyroxenitic komatiite has been recognized in this area. The limited occurrence of komatiites makes detailed discussion of their generation difficult. Nevertheless, the constant near-chondritic Zr/Y ratios (Fig. 2.6) suggests that garnet was not involved as a residual phase when komatiite was produced in this area, since Y would partition strongly into the garnet (c.f. St.Seymour et al. 1983).

2.5 Relationship of the komatiite to the basalt

The intimate spatial relationship of the komatiite to the basalt and their similar trace element ratios suggest that they may be genetically related. The low Mg#s of the basalts make it unlikely that they represent primary magmas (Fig.2.4). It is possible that the komatiites represent the parental magmas from which the basalts were produced by fractionation. However,

quantitative modelling, using both fractional crystallization and equilibrium crystallization calculations, fails to yield the high-Mg basalt from the komatiite. One of the closest approaches, by fractionating olivine and orthopyroxene, is presented in Table. 2.4. The high TiO2 and FeO may reflect the absence of an oxide phase in the model and the low Na2O may simply reflect alteration of the Na2O contents in the komatiites. The real problem is Al2O3: it is impossible to raise Al2O3 from 6.80% in the komatiite to 16.79% in the high-Mg basalt by fractionating reasonable mineral assemblages. (Although fractionating clinopyroxene would increase Al in the melts, it would greatly decrease Ca at the same time.). Calculations using the pyroxenitic komatiite in Lac Guyer area as the parental magma meet with the same problem. It seems that the parental magma to the high-Mg basalt had a higher Al/Si ratio than that of the komatiite.

In Al-Si space, most modern picrite suites define linear arrays projecting away from olivine (Francis et al. 1983), reflecting olivine controlled crystal fractionation. Thus, if we suppose the high-Mg basalt was derived from a picritic magma(s), this parental magma is likely to have had a higher Al/Si ratio, on the line connecting olivine and the high-Mg basalt in Al-Si space (Fig. 2.8). One possible relationship of this postulated parental magma to the komatiite is that it reflects a lower degree of adiabatic partial-melting at a greater depth (see Fig. 2.8), at an earlier stage of the development of a rising mantle

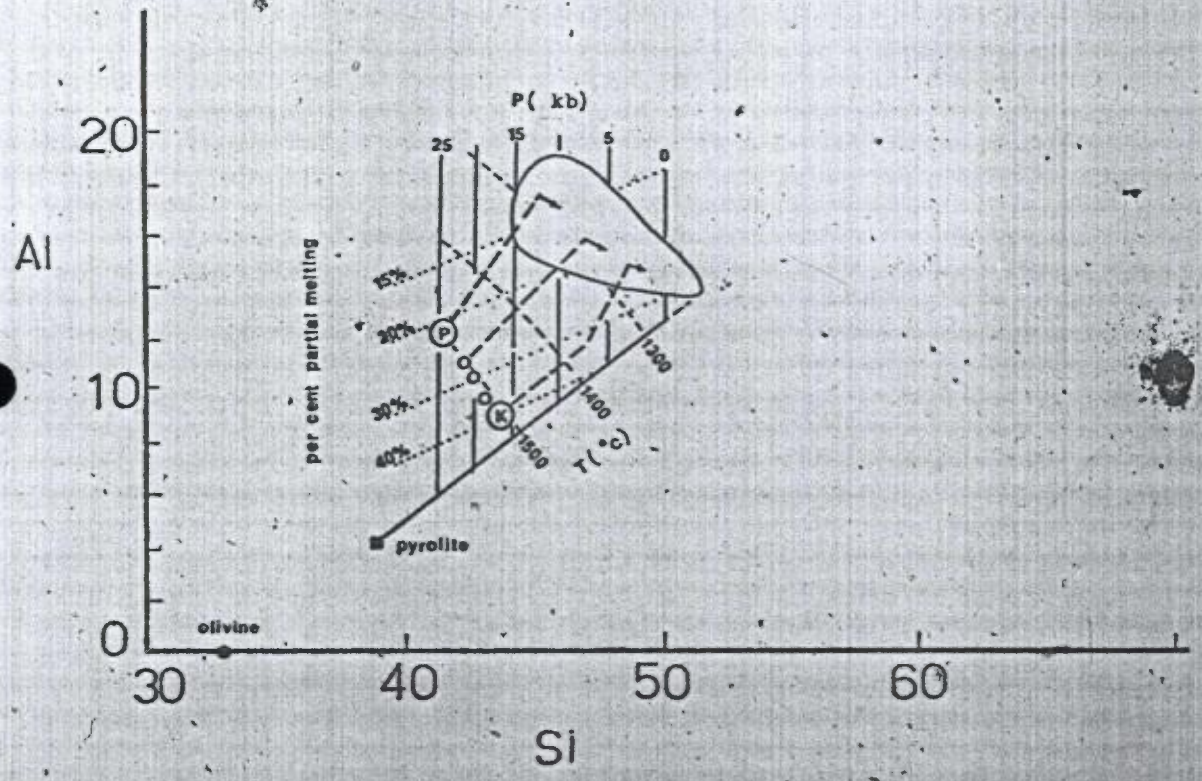
P(kb)
25
15
1
5
0
15%
20%
30%
40%
per cent partial melting
P
K
1200
1400
1500
T(°C)
pyrolite
olivine
Al
20
10
0
30
40
50
60
Si

Fig. 2.8

diapir. As the diapir rose, decrease of pressure may have caused more partial-melting to yield the komatiite at shallower depth. This process is similar to the multi-stage melting model of Duncan and Green (1980) and to the case of the Cape Smith fold-belt (Francis et al. 1983).

There are some alternative possibilities, including: (1) The high-Mg basalts were directly derived from the mantle by partial melting. The location of the initial-melt line in Figure 2.4 is very sensitive to the composition of the mantle, of which our knowledge is still very poor. If the mantle was more Fe-rich than assumed in Figure 2.4, the initial-melt line would be lower and the high-Mg basalts could lie within the primitive melt field. (2) The komatiite and basalt were derived from different mantle sources, reflecting the heterogeneous nature of the mantle. These possibilities, although not favoured in this study, cannot be completely ruled out.

Fig. 2.8. The postulated relationship of the komatiite (the circled K) to the magma parental to the high-Mg basalt (circled P) during increasing degrees of abiabatic partial melting, presented in Al-Si space (in cation units). The open circles are the possible primary magmas. The dashed lines with arrows show the possible paths producing basalts from the primary magmas by crystal fractionation. The T-P-percent melting grid is adapted from Francis et al. (1983).

2.6 Tectonic evolution

The chemical development of mafic magmas is controlled largely by physical conditions which are in turn controlled by the tectonic evolution. The MORB-like major element characteristics, the abnormal Rb and K contents and the stratigraphy all indicate an Archean tectonic setting analagous to modern continental rifting (c.f. Nesbitt and Sun 1976; Hynes and Francis 1982; Dupuy and Dostal 1984). The relatively large volume of the first-sequence basalt may reflect a large magma reservoir built up under a strong continental filter, at an early stage of rifting. Continuous rifting may have weakened this filter and the second-sequence basalt erupted before a large volume of magma could accumulate. With further opening, the continental filter collapsed and komatiites erupted. This process is similar to the crust-filter model proposed by Francis et al. (1983) for the magmatic evolution of the Cape Smith foldbelt.

In the western part of this greenstone-belt (Skulski et al. 1984; Rivard and Francis 1984), the basalts probably fractionated at a lower pressure than the basalt in the study area, as indicated by their relative positions in the Di-Ol-Sil pseudo-liquidus phase diagram (Fig.2.9). This diagram is very sensitive to the alkali (CaO, Na2O and K2O) content of the rocks (see Elthon 1983). The relatively high alkali content in the basalts of the western part (Fig.2.10) shifts these data towards Ol. Adjustment for this would lead to an even greater decrease in

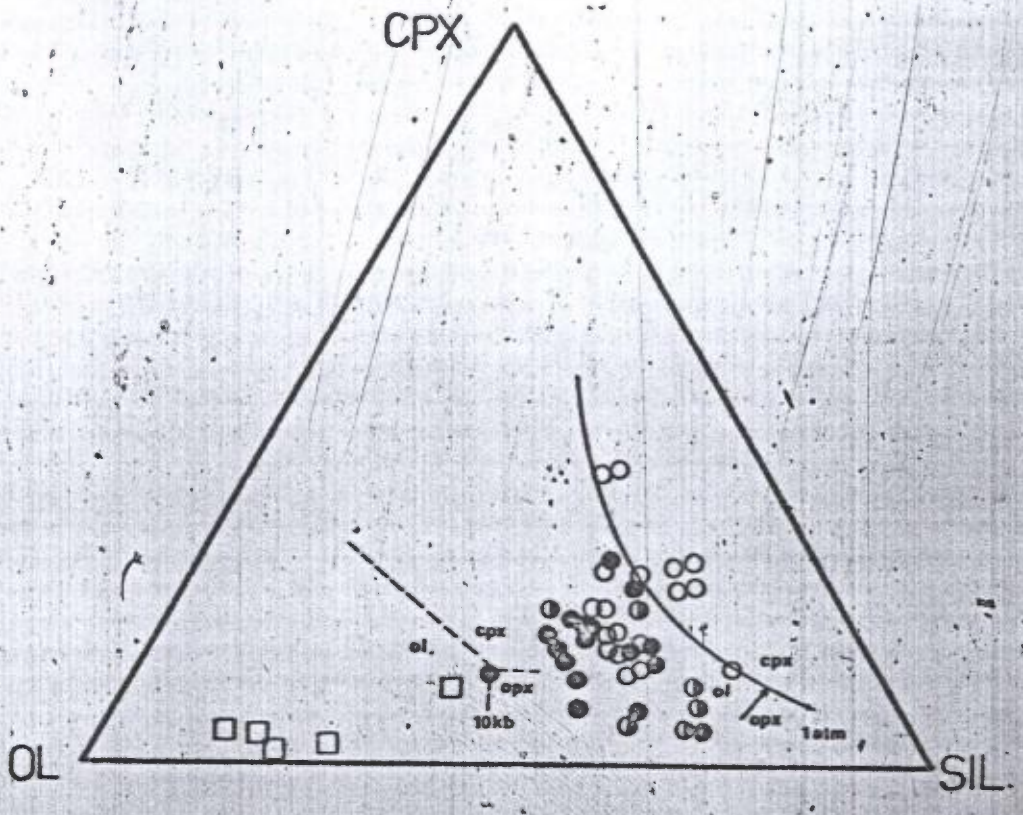

Fig. 2.9

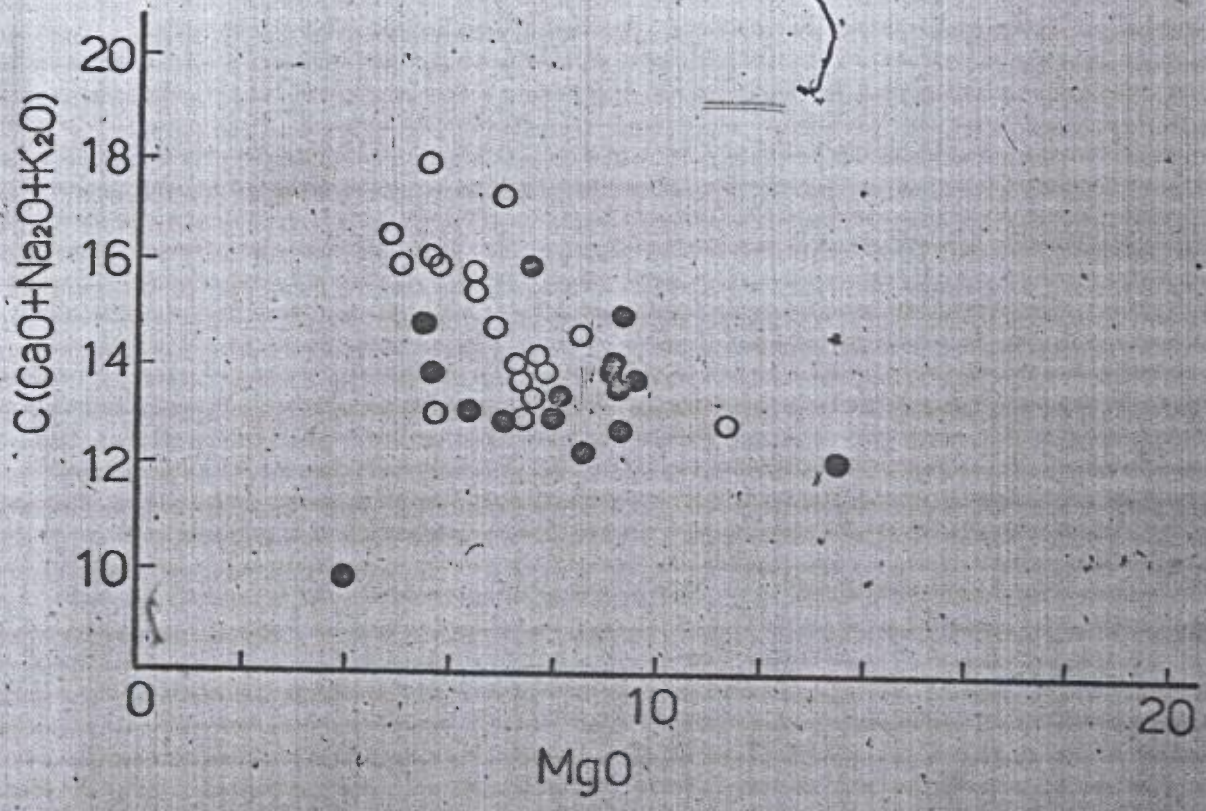

Fig. 2.10

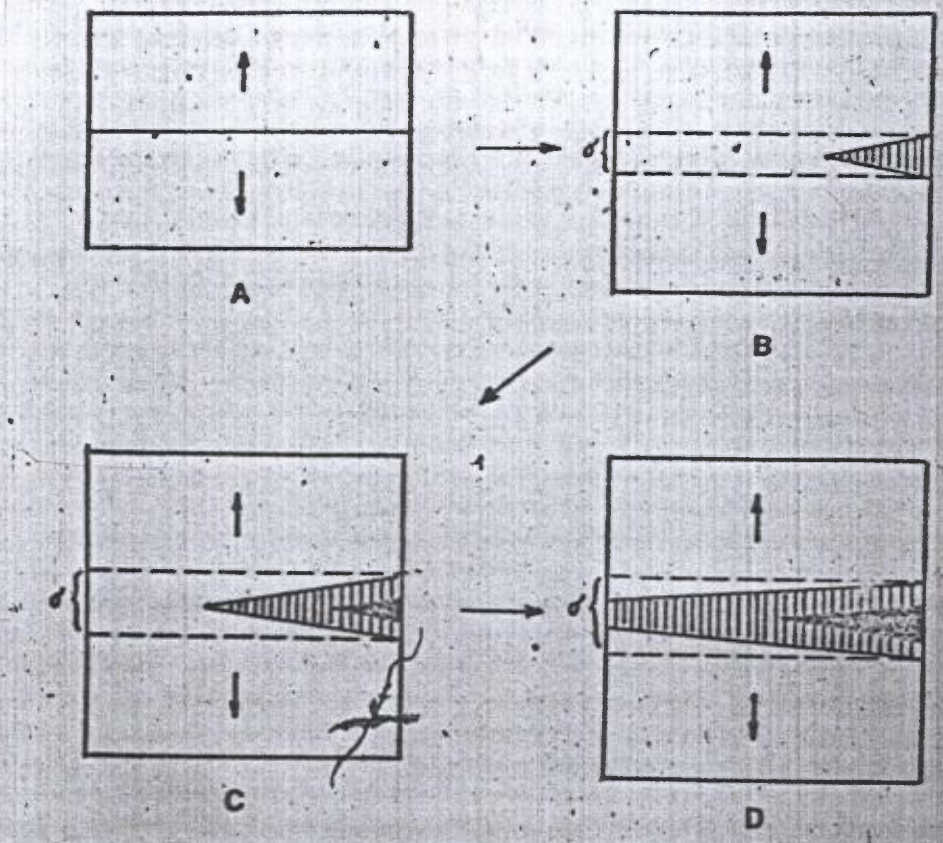

Fig. 2.11

Fig. 2.9. Isomolar pseudo-liquidus phase diagram for the La Grande greenstone-belt after Elthon (1983,1984). Solid circles and squares as in Fig.2.2. Half filled circles are the basalts from LG3 area (Skulski et al. 1984). Open circles are basalts from LG2 area (Rivard and Francis 1984). Notice that the basalts from LG2 area are generally concentrated along the 1 atm cotectic line while the cotectic line for the basalts in the study area lies somewhere between the 1 atm and 10 kb cotectic lines. The basalts from LG3 area are between those of LG2 area and the study area.

Fig. 2.10. C (CaO + Na2O + K2O) vs. MgO for the La Grande greenstone-belt. Symbols as in Fig.2.9.

Fig. 2.11. Rifting-propagation model for the evolution of La Grande greenstone-belt. A: before rifting. B: rifting started from the east, causing the eruption of basic magma in Lac Guyer area and the study area. The crust in front of the rift was undergoing extension and thinning. σ show the amount of extension caused by the rifting. C & D: the rifting propagated to the west, causing the eruption of basic magma in LG3 and LG2 areas. Behind the rift the crust collapsed and komatiitic magma erupted in Lac Guyer area and the study area.

pressure with progress to the west. This, together with the relative proportions of komatiites, which decrease from the Lac Guyer area to the study area and are absent in the western part of the belt, may indicate a rifting-propogation process for the evolution of the La Grande greenstone belt (Fig. 2.11). The magma body located to the east, eruption of basic magma derived from a magma reservoir under a relatively thick continental crust started here. At the same time the crust in front of the rift was undergoing thinning and extension (see Vink 1982). Further opening propagated the rifting to the west and caused the eruption of basic magma from a thinned crust, while behind the rifting the continental crust collapsed and komatiites were erupted.

2.7 Conclusions

Geochemical study of the La Grande greenstone belt suggests that it developed in an Archean rifting environment. Two sequences of basalt erupted through continental crust at the early stages of the rifting, followed by the eruption of komatiites. Evolution of the basaltic magmas may have been controlled by crystal fractionation of olivine, pyroxene and plagioclase. The actual fractionation process was probably somewhere between fractional crystallization and equilibrium crystallization, with most olivine crystals removed from the magma while plagioclase and some pyroxene crystals remained. The

abnormal behavior of Rb and K may be due to contamination by continental crust when the magmas passed through it.

The komatiites, with their high MgO content, probably reflect large degrees of partial-melting of the mantle. Despite their intimate spatial relationship to the basalt and their similar trace element ratios, the komatiites cannot be the direct parental magmas to the basalt. However, the generation of komatiites could possibly be similar to that of the parental magma to the basalt, differing only in its greater degree of adiabatic partial-melting at possibly shallower depth. The parental magma to the basalt may have last equlibrated with the mantle under a relatively thick continental crust. As the mantle diapir rose, decrease in pressure may have caused increasing adiabatic partial-melting and thus produced komatiitic magma, which then erupted through newly-formed oceanic crust at a later stage of the rifting.

A model of rift-propagation from east to west is proposed for the La Grande River greenstone-belt to account for the observations: (1) The basic magma fractionated at a higher pressure in the eastern part of the greenstone belt than in the western part; (2) Komatiites decrease in volume from Lac Guyer area to the study area and are absent in the western part of the greenstone belt.

This chapter presents only a preliminary study of the volcanic petrogenesis in the greenstone belt. There are many

problems remaining with the evolution of this belt. The lower Fe concentration in the high-Mg basalt than in the komatiite requires fractionation of magnetite during its generation from the parental magma, which would probably have had an even higher Fe concentration than the komatiite since it represents a lower degree of partial melting (see Hanson and Langmuir 1978). Study of the basalt in the western part of the belt (Rivard and Francis 1984), however, has shown that magnetite fractionation probably occurred during evolution of the basalt suite there, producing an Fe-depletion trend opposite to that of the basalt in this area (Fig. 2.4). This may be controlled by variation in fO2. The attainment of high fO2 at different stages of magma evolution in the eastern part and western part of this greenstone belt may possibly be related to variations in the mantle degassing mechanism during the rifting process (c.f. Mathez 1984).

Table 2.1. Geochemistry of volcanic rocks in the La Grande greenstone belt

	Komatiite			High-Mg basalt			Low-Mg basalt		
	039	040	052	062	068	082	066	067	079
SiO2	44.58	44.74	46.30	49.24	49.61	49.97	51.37	52.95	50.52
TiO2	0.50	0.32	0.48	0.70	0.43	0.72	1.17	1.86	1.15
Al2O3	6.79	6.81	7.06	16.98	16.92	15.30	14.89	12.30	12.90
MgO	27.51	28.70	26.73	9.29	9.12	9.09	6.38	3.96	5.55
FeO	15.11	13.18	13.69	10.78	8.58	10.57	12.80	18.60	12.90
MnO	0.19	0.20	0.23	0.18	0.15	0.18	0.24	0.36	0.20
CaO	5.24	5.90	5.39	8.98	8.58	10.57	11.21	7.09	11.94
Na2O	0.03	0.06	0.08	2.21	1.24	1.83	1.63	2.62	1.69
K2O	0.01	0.01	0.01	1.59	1.44	0.19	0.14	0.24	0.16
P2O5	0.04	0.04	0.03	0.05	0.02	0.03	0.07	0.10	0.07
Mg# (Mg/Mg+Fe*)	0.79	0.82	0.80	0.64	0.70	0.64	0.50	0.29	0.46
Cr	3234.1	245.9	3125.4	247.8	766.8	395.1	61.8	120.3	150.2
Ni	86.4	829.0	852.2	148.3	81.7	89.3	53.4	7.9	38.2
Zr	29.0	16.3	23.0	32.8	16.6	37.0	54.5	78.2	51.4
Y	12.8	8.9	10.7	15.2	10.4	15.7	24.0	36.6	24.2
Rb	1.5	1.2	2.0	87.3	73.9	3.7	3.6	3.6	2.4

sur 100%

Voir annexe pour les valeurs originales

✓ ✓

Table 2.2. Major Element Crystallization Calculation

	High-Mg basalt	Low-Mg basalt	Cl'(1)	Cl'(2)	Δ(1)	Δ(2)
SiO2	48.96	51.00	51.33	51.01	0.006	0.000
TiO2	0.56	1.37	1.00	0.99	-0.270	-0.277
Al2O3	16.79	14.14	14.43	14.42	0.021	0.020
MgO	9.12	5.22	5.35	5.63	0.025	0.079
FeO*	9.59	14.56	13.89	10.20	-0.460	-0.299
CaO	10.63	9.95	8.47	9.29	-0.149	-0.066
Na2O	1.71	1.95	2.08	1.86	0.067	-0.046

Table 2.3. Trace Element Crystallization Calculation (in ppm)

	Low-Mg basalt	High-Mg basalt	C'o(1)	C'o(2)	Δ(1)	Δ(2)
Zr	61.37	33.94	31.29	31.90	-0.078	-0.060
Y	28.00	15.92	15.20	15.65	-0.045	-0.017
Ti	10033.33	5008.00	5328.50	5544.72	0.064	0.107
Cr	130.31	411.87	262.41	172.45	-0.363	-0.581
Ni	40.20	115.00	160.80	82.16	0.398	-0.286

Table 2.4. Calculation of Fractional Crystallization

	Komatiite	High-Mg basalt	Daughter magma	Relative error
SiO2	44.62	48.96	48.42	-0.01
TiO2	0.43	0.56	0.87	0.55
Al2O3	6.80	16.79	13.57	-0.20
MgO	27.29	9.12	9.26	0.01
FeO*	13.81	9.59	15.56	0.62
CaO	5.44	10.63	11.02	0.04
Na2O	0.06	1.71	0.12	0.93

Table. 2.1. All the elements were determined by XRF at the Department of Geological Sciences, McGill University. The major elements are normalized to one hundred percent volatile-free with total Fe calculated as FeO. See Appendix-I for analytical methods.

Tab.2.2. " High-Mg basalt" is the average of 5 basalts with MgO content around 9%. " Low-Mg basalt" represents the average composition of 4 basalts with MgO around 5-6%. The crystallization calculations were performed with a finite-difference computer technique (c.f. Nathan and Van Kirk 1978; Cox 1980). The program for fractional crystallization repeatedly calculates the instantaneous equilibrium compositions of crystals coexisting with the liquid, with removel of these phases in a quantity of 0.01 cation percent of the initial parent at each step and recalculates the residual liquid to 100 percent. The composition of olivine was obtained using the distribution coefficient of Roeder and Emslie (1970). The KD of Mg/Fe in clinopyroxene was according to Camble and Taylor (1980). Other components of clinopyroxene were taken from the composition of low alkali basalt (Leterrier et al. 1982). The composition of plagioclase was calculated according to Nathan and Van Kirk's (1978) formula. The program for equilibrium crystallization is similar but simpler. Instead of removing the crystals in finite steps, it performs a simple mass-balance calculation. Mineral proportions were firstly estimated from the low pressure cotectics and then adjusted duiring the calculation to obtain the best fit to the observed rock compositions. Cl(1) is the composition of daughter

magma derived by fractional crystallization. olivine, clinopyroxene and plagioclase were fractionated in the cation proportions 26/20/54 until 50% of the original liquid remained. Cl(2) was obtained by equilibrium crystallization. Olivine, clinopyroxene and plagioclase were crystallized in the proportions 28/16/56 until 51% of the original liquid remained. $\Delta(1)$ and $\Delta(2)$ are the relative errors for the fractionation crystallization and equilibrium crystallization models, respectively. The equation for fractional crystallization is: $Co/Cl = F^{(D-1)}$ where Co and Cl are the element concentrations in the original and daughter magma, respectively, D is bulk the distribution coefficient of the element between the crystals and the magma and F is the fraction of the original melt remaining. The equation for equilibrium crystallization is $Cl/Co = 1/(D(1-F) + F)$. The symbols are the same as in the equation of fractional crystallization except that here F represents the fraction of crystals crystallized.

Tab. 2.3. C'o(1) and C'o(2) are the element concentrations in the parental liquid calculated by fractional-crystallization modelling and equilibrium-crystallization modelling, respectively. Parameters used in this calculation were taken from Table 2.2 and the D's were determined by the mineral proportions in the major-element modelling and mineral/liquid distribution coefficients of the elements from Pearce and Norry (1979) and Cox and Pankhurst (1979). $\Delta(1)$ and $\Delta(2)$ as in Table 2.2.

Table. 2.4. The komatiite composition is the average of samples 039,040,052. The daughter magma was derived by fractional crystallization modelling. In this calculation olivine was fractionated alone until the MgO content in the liquid was below 12%, then olivine and orthopyroxene were fractionated in cation proportions 20/80 until 53% of the original magma was fractionated.

Chapter 3

MIGMATIZATION IN THE GNEISSIC-GRANITIC TERRANE

Migmatization is widespread in the gneissic-granitic terrane which surrounds the greenstone belt. In recent years quantitative mass-balance studies have greatly improved our understanding of migmatization (Olsen 1977, 1983, 1984). If the composition of the parental rock to migmatite is known, the proportion of leucosome to restite required for a closed system may be obtained by least-squares calculation. Comparing this ratio with that measured from the rocks, Olsen (1977, 1983) showed that migmatization occurred in a system essentially closed except for volatile components. This was in accordance with the observations of Mehnert (1968). Olsen's (1984) recent work on the migmatites in the Colorado Front Range, however, revealed some mass transfers, particularly the gain of K and loss of Na and Mg by the system. These calculations were limited to low grade migmatites, in which the leucosome and restite were clearly distinct, but in direct contact with each other. For high grade migmatite, little work has been done. This is mainly because the restites that co-existed with the granitic leucosomes are generally not observed in the field. They were left behind when the granitic leucosomes were extracted. In this case Olsen's method is not applicable.

In this chapter migmatization in the gneissic-granitic terrane is discussed. A 1500 metre road cut in the study area

shows a clear gradation from biotite gneiss, which was not affected by the migmatization, through metatexite and diatexite to homogeneous granite, providing a good opportunity to study progressive migmatization. (Terminology is after Mehnert, 1968. Metatexite is heterogeneous, with distinct leucosome and melanosome, typical of low-grade migmatite. Diatexite is more homogeneous and higher grade. However, there is no sharp boundary between them). Because of the progressive character of the migmatization, it is possible to obtain an estimate of the composition of the parent rock even for the high-grade migmatites, provided the degree of migmatization was controlled by temperature rather than bulk-chemical differences. It is shown here that the continuous variation of the migmatites observed on the outcrop does reflect a mainly temperature-controlled migmatization gradient. Mass transfer during migmatization is then studied using a simple mass-balance calculation for each major component, with the estimated restite compositions based on the experimental results of Winkler (1979).

3.1 General geology and petrography

The gneissic-granitic terrane studied is in the south of the greenstone belt (Appendix-V). The roadcut discussed in this chapter occurs along the LG3-LG4 highway, about 80 kilometres west of LG4. Westwards along the outcrop, the rocks change gradually from apparently homogeneous, fine grained biotite gneiss to metatexite, with distinct separation of the felsic

A

plate 3.1

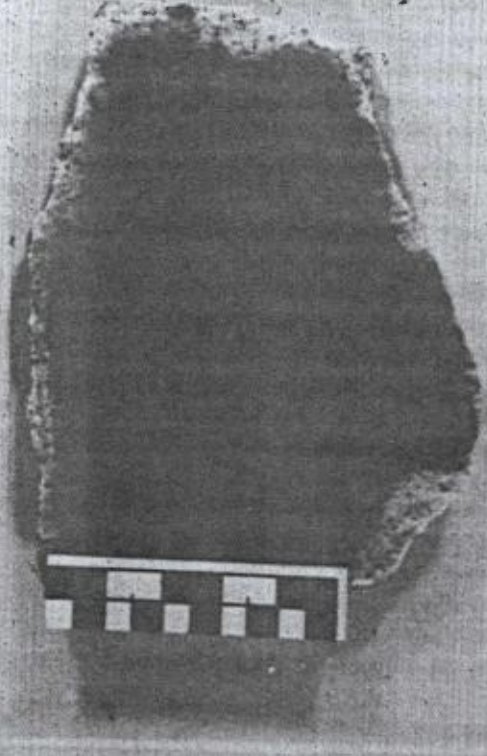

B

C

phases from the biotite, which is recrystallized to coarse flakes. The rock then progresses to diatexite, with a clear decrease of the dark components. Further west the rock changes to homogeneous, pinkish granite. There is no evidence of a structural break along the outcrop. A brief description of the petrography of the rocks follows.

Biotite paragneiss: The mineral assemblage is quartz(25%), plagioclase(40%), biotite(30%) and a little pinkish garnet. No potassium feldspar has been found. The felsic grains are flattened and separated by biotite bands, which conform to the regional foliation. Some layers of conglomerate indicate a sedimentary origin.

Metatexite (Plate.3.2A): The mineral assemblage is quartz(20-25%), plagioclase(35-40%), biotite(30-35%) and some garnet and apatite. Potassium feldspar is rarely found. Plagioclase grains are generally subhedral, with margins commonly embayed by quartz. Distinct leucosomes and biotite-rich restites are present and the leucosomes are commonly surrounded by dark rims of recrystallized biotite.

Plate.3.1. Migmatites. A: Metatexite. The leucosome is surrounded by recrystallized biotite. B: Diatexite. Restite cannot be easily recognized. C: Anatectic granite. The rock is almost homogeneous.

Diatexite (Plate.3.2B): The mineral assemblage is potassium feldspar (25-30%, mainly microcline), plagioclase(30-35%), quartz(20-25%) and biotite(10-15%). Plagioclase grains are subhedral to anhedral. Some are skeletal, embayed by quartz. Leucosome and restite are not easily distinguished.

Granite (Plate.3.2C): The mineral assemblage is potassium feldspar(40%), quartz(30%), plagioclase(25%), and biotite(5%). Perthite megacrysts are common. It is more homogeneous than diatexite and has an interlobate granoblastic texture.

3.2 Controls of migmatization

The gradation of migmatitization observed on the outcrop could reflect a temperature gradient, compositional variation of the rocks, or a combination. Several features suggest that the temperature gradient was the dominant control: (1) Feldspar-geothermometry shows a clear temperature gradient along the outcrop (Fig. 3.1). Although the general low temperature in Figure 3.1 indicates that the feldspar is affected by subsolidus re-equilibration to a certain degree, the trend of temperature increasing from low grade migmatite to migmatized granite is still preserved. (2) The compositions of plagioclase in the biotite-paragneiss, the leucosome of metatexite and granite are: Ab62 An27 Or1, Ab72 An27 Or1 and Ab86 An13 Or1, respectively. This is in accordance with the plagioclase-melting experiment of

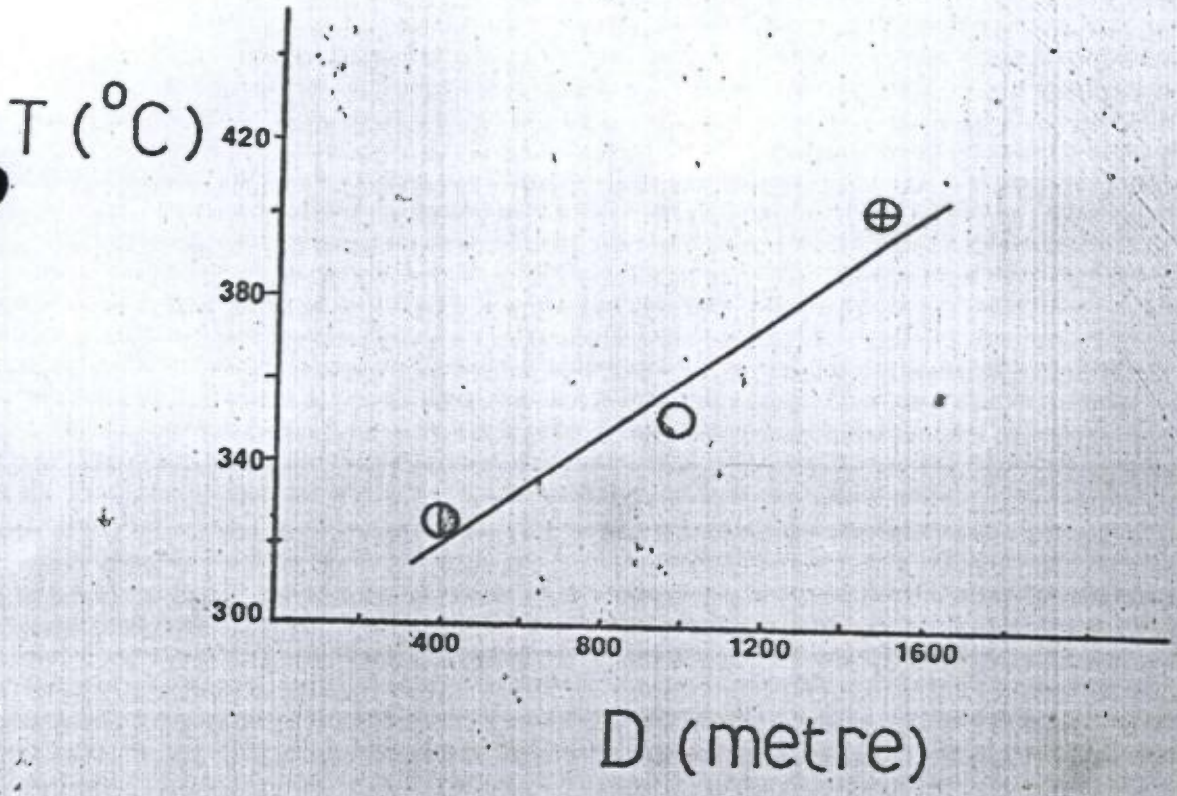

Fig. 3.1

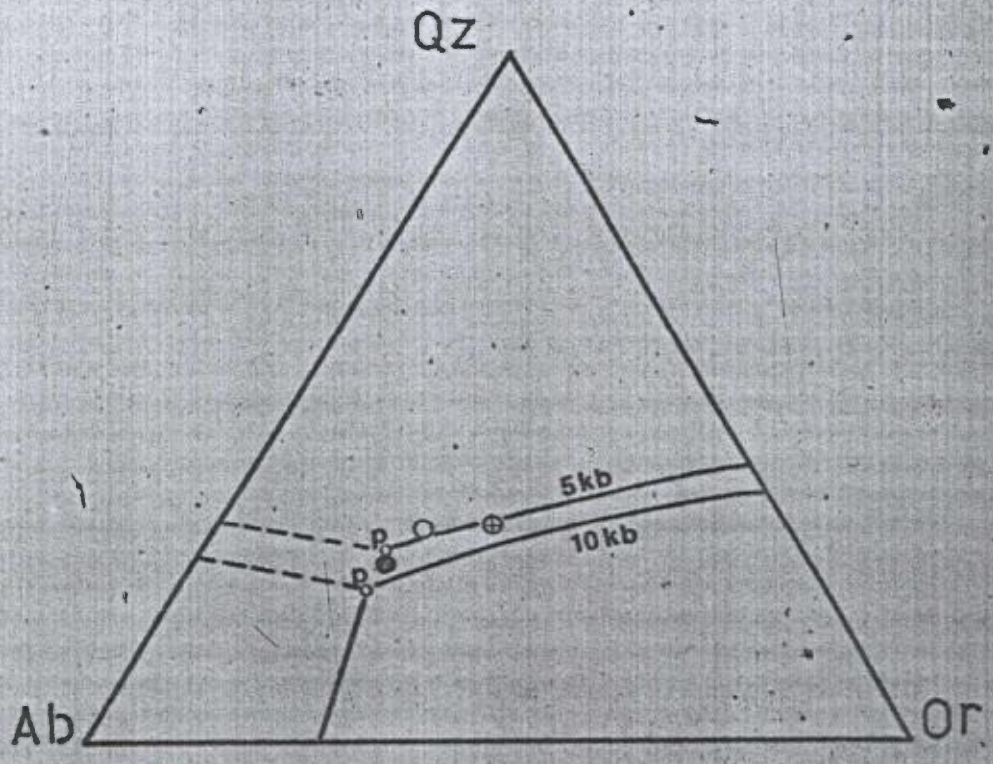

Fig. 3.2

Fig.3.1. Average temperature of the migmatites as a function of the distance away from the biotite gneiss along the outcrop. Half filled circle--metatexite; open circle-- diatexite; circled cross--anatectic granite. Temperature was obtained using Whitney and Stormer's (1977) feldspar geothermometer.

Fig. 3.2. Normative composition in the Qz-Ab-Or ternary field. Solid circle represents the biotite gneiss. Other symbols as in Fig.3.3. Eutectic points, P, represent the "minimum melt". Cotectic lines adapted from Luth et al.(1964).

Drake (1976), who showed that, during anatexis, the albite component of plagioclase would fractionate strongly into the melt, and that the distribution coefficient of Na between the melt and plagioclase increases with temperature. (3) The textures of the leucosomes indicate a gradual increase of degrees of partial melting from metatexites to granites. The plagioclase grains in metatexite are commonly subhedral and embayed by quartz, suggesting the early melting of quartz. This phenomenon is better developed in the diatexite. In the granites, the interlobate granoblastic texture indicates almost complete melting of the felsic components and relatively rapid crystallization. (4) The composition of biotite gneiss is very close to that of the "minimum melt" (Fig. 3.2). It is therefore very unlikely that the absence of migmatization at the eastern end of the road cut reflects refractory characteristics of the rocks there.

The outcrop thus provides a good opportunity for studies of progressive migmatization and the composition of the biotite gneiss may be used as a reasonable estimation of that of the parent rock of the high-grade migmatites for mass transfer studies.

Among the mechanisms proposed for migmatization, four are generally accepted: (1) partial melting; (2) metamorphic differentiation; (3) lit-par-lit injection of a granitic magma; (4) metasomatism. (see Yardley 1978). The above discussion indicates that partial melting played an important role in the

migmatization of this terrane. In the following mass balance studies we shall see if partial melting alone can account for the observed migmatization.

3.3 Mass transfer in migmatization

The composition of the parental rock of migmatite must be known in order to study mass transfer in migmatization. In most previous studies the part of migmatite least affected by migmatization (so called "paleosome") was taken as the original rock (e.g. see Mehnert 1968; p.250, Olsen 1984). Although in many cases this is the only possible choice, it is doubtful that the paleosome reflects the true composition of the parental rock. The paleosome is commonly in contact with the more migmatized part (leucosome + restite) on a scale of a few centimetres. Since it is not likely that the degree of migmatization would vary significantly on such a small scale, the preservation of the paleosome is best explained as due to compositional differences (see Johannes and Gupta 1982). In this study, however, the biotite gneiss may be used as a guide to the composition of the original rock for reasons discussed above.

For a closer comparison with possible volume changes, cation units have been used in the following mass balance calculations. Table 3.1 presents the bulk compositions in terms of eight major components: Si, Ti, Al, Fe* (total iron), Mg, Ca, Na, and K, normalized to 100 percent.

For the metatexite, in which the leucosome veins are commonly less than 0.5 cm thick, two 1000 cm^3 samples were ground and analysed (Tab.3.1). The average composition is very close to that of the biotite paragneiss. Considering the errors in the analysis, the metatexite may be regarded as having formed in a closed system (c.f. Olsen 1977, 1982), although there may be a slight gain of Si and loss of Fe* and Mg.

For the higher grade migmatites, the diatexite and anatectic granite, mass transfer of each component is considered separately. Since no strong correlation exists among the components, fitting the whole matrix by a least-squres method such as that used by Olsen (1984) is not useful here.

Assuming closed-system anatexis, an equation of mass balance can be established:

$$100C_p^i = Xc\, C_m^i + (100 - Xc)\, C_r^i \qquad (1)$$

where Xc is the percentage of partial melting and C_m^i, C_r^i and C_p^i are the concentrations of component i in the melt, restite and parental rock, respectively. The test for a closed system is very simple: the values of Xc derived from equation (1) for each component should be the same or at least very close. The diatexite and anatectic granite may be treated as approximations to the melt compositions. Although they may not have formed completely from the melts, Xc may in this case be regarded as the

percentage of the neosome of the migmatite and the test is not affected. The problem here, however, is to identify the composition of the restite, which is not apparent in the field. Winkler's (1979) melting experiment on biotite paragneiss showed that, at high degrees of partial melting, the restite was dominated by biotite. Consequently, in a first test, the composition of the biotite in the diatexite and migmatized granite was taken as that of the restite. The values of Xc for eight major components obtained with this assumption vary greatly (Tab.3.2). Xc for K, Ca, and Na, in particular, are physically unrealistic (>100%). Thus, the migmatization is unlikely to have occurred in a closed system. Another test, using a model restite (Bio70 Pl15 Qz10 Gar5) supports this conclusion (Tab.2). The high Xc values for K, for example, arise because the K content in the anatectic granite(6.34 cat.%) is higher than in the biotite gneiss (2.91 cat.%); a closed-system would therefore require the K content in the restite to be lower than that in the biotite gneiss. This means biotite, the major K-bearing mineral phase in the restite, would have to be lower than 27% in the restite and the amount of partial melting for the generation of the anatectic granite would have to be lower than 45%. Neither of these conditions is easily fulfilled, so that the conclusion of an open system is therefore unlikely to be changed with other reasonable choices of restite composition.

For an open system, equation (1) is changed to:

$$100\ C'^{i}_{p} = Xo\ C^{i}_{m} + (100 - Xc)\ C^{i}_{r} \qquad (2)$$

Here Xo is the actual amount of partial melting in the open system and C'^{i}_{p} the concentration of component i in the net (melt + restite) migmatite. Thus the amount of a component gained or lost by the system, D_i, may be obtained from:

$$D_i = C'^{i}_{p} - C^{i}_{p} \qquad (3)$$

In this calculation we need to know the values of Xo. If it can be proved that the system was actually closed to one of the components, or in other words, that this component was completely immobile, the value of Xo can obtained. In this case Xo is equal to Xc, which can be calculated from equation (1). Unfortunately, none of the components can be proved to be completely immobile. Nevertheless, a reasonable range of Xo may be estimated and the results are insensitive to variations in it (see below). Melting experiments on a Qz-Pl-Bio-Ksp paragneiss at PH2O = 5 Kb showed that, by about 45 °C above the solidus temperature, 65-75% of the rock was melted (Winkler 1979). Figure 3.1 shows that the anatectic temperature of the migmatized granite was at least 80 °C higher than that of the low grade migmatite. It may therefore be expected that Xo for the anatectic granite and diatexite was high. The amount of partial melting also depends on the composition of the original rocks. Since the parent rock in this study is compositionally very close to the "minimum melt" in the normative Qz-Or-Ab ternary field (Fig. 3.2), a large amount of partial melting would be expected within a small range of temperature above the solidus. In the mass-

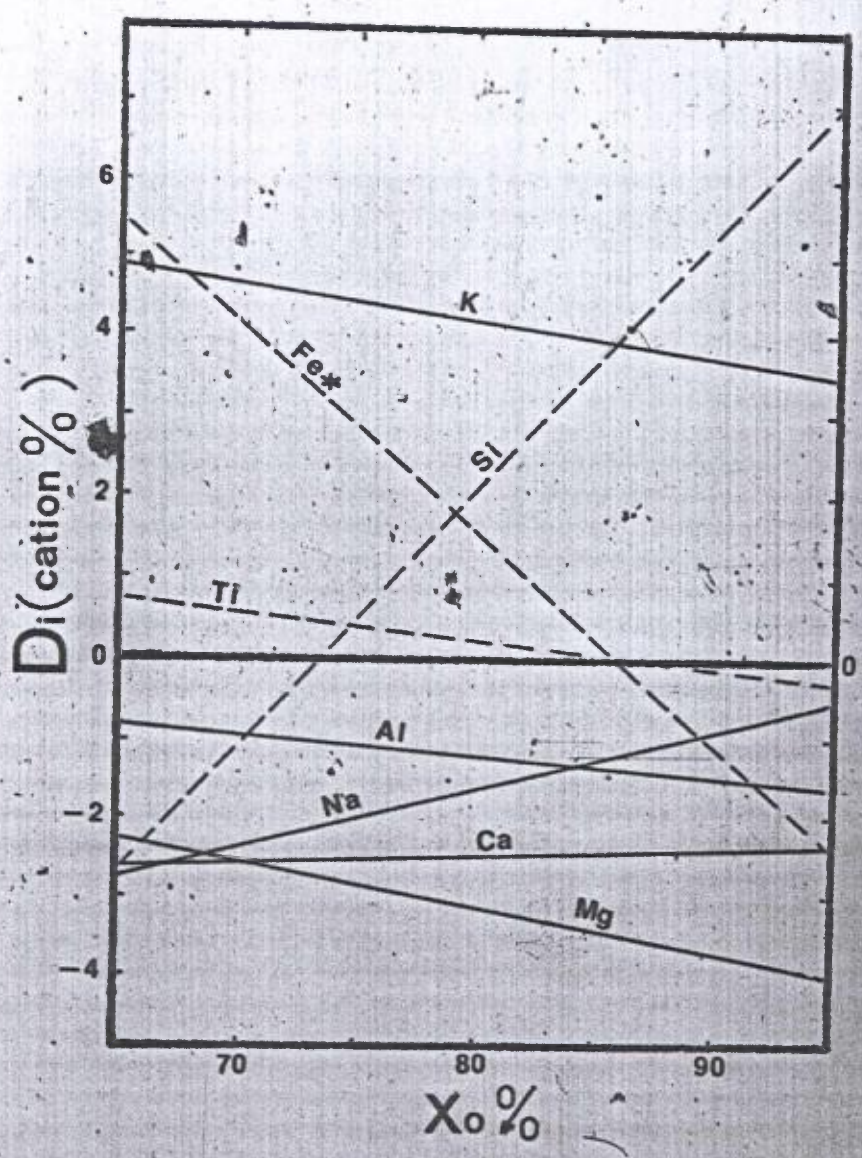

Fig. 3.3

balance calculations for the generation of diatexite and granite, values of Xo in the range from 65% to 95% were considered. The results are presented in Table 3.3 and in Figure 3.3.

For discussion of the mass transfer, the eight major components are divided into three groups:

(1) K, Ca, Na : These three components were almost certainly mobile during formation of the granite. In all the physically possible range of Xo (from 0 to 100%), K must be gained and Ca and Na lost by the system (Tab. 3.3). The same is true for the formation of the diatexite, except for Na. The mass transfer of Na at this stage is not clear. This is because its Xc value is in the range estimated for Xo, thus the exact value of Xo must be available to determine whether Na was gained or lost.

(2) Al, Mg: These two components were lost at both diatexite and granite stages for the reasonable choices of Xo. The loss is greater for model-B restite(Bio70 Pl15 Qz10 Gar5) than for the model-A restite (pure biotite; Tab.3.3). Gain of Mg

---

Fig. 3.3. Mass transfer (in cation percent) in formation of the anatectic granite as a function of the degree of partial melting, with restite as pure biotite. Dashed lines are for the components whose mass-transfer are uncertain within the considered range of Xo. c.f. Tab. 3.3.

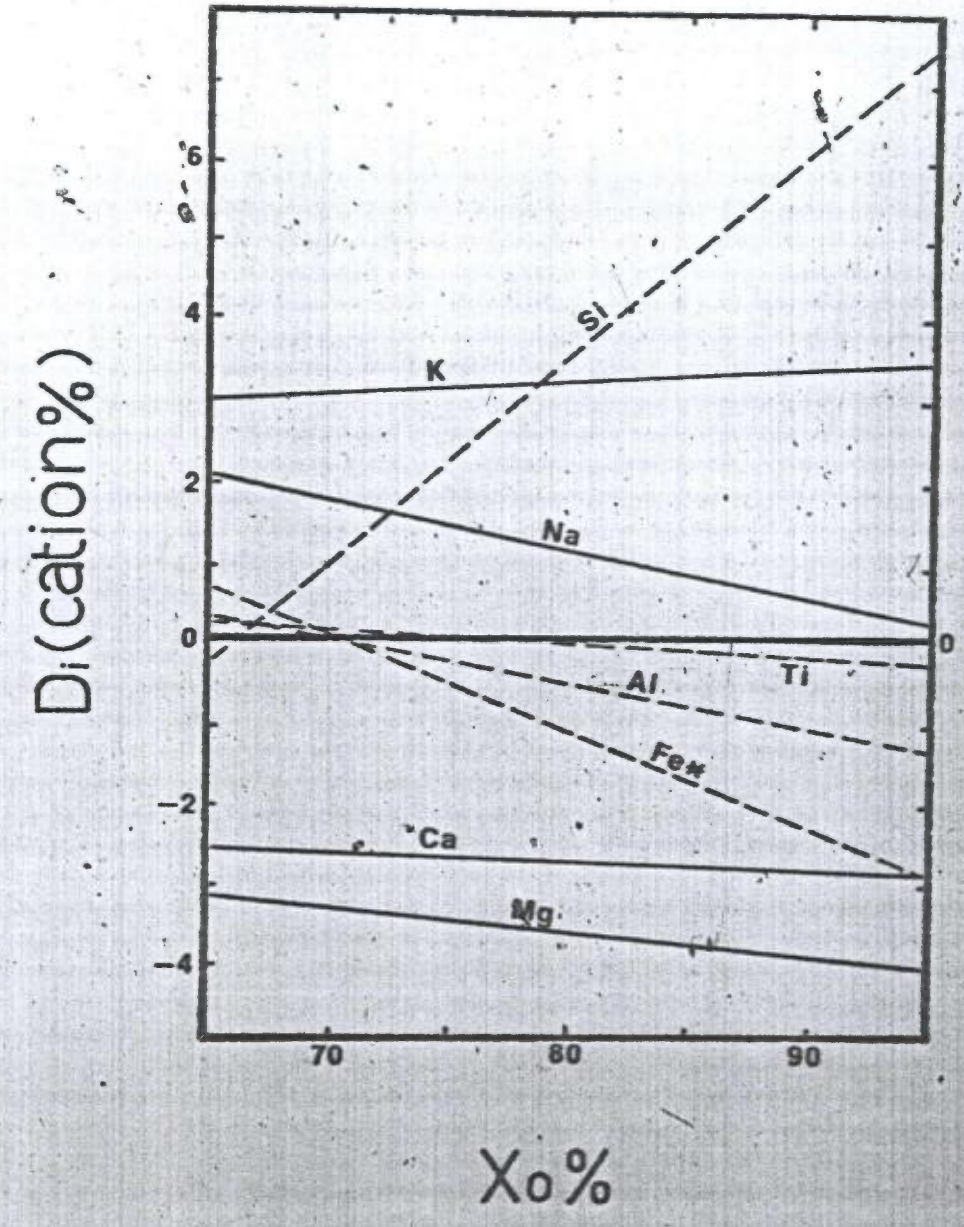

Fig. 3.4

by the system would be possible for model-A restite only if the value of Xo was below that of Xc (49% for diatexite and 27% for granite. c.f. Tab.3.2). The case for Al is similar.

(3) Si, Ti, Fe*: The status of mass transfer for these components is not clear, since their Xc values are all in the possible range of Xo. Assuming 80% partial melting for the formation of granite, Si, Ti and Fe* are gained by the system. However, no firm conclusion may be drawn without precise values for Xo.

The mass transfers dicussed above are clearly affected by the choice of restite composition. Although in the restite there were possibly some other minerals, such as cordierite and hornblende, which might be produced during anatexis, their proportions are likely very small (Winkler, 1979) and would not have an important influence on the mass-balance studies. Error could, however, come from plagioclase, which may have had higher proportions in the restite than those used in the calculations above. Figure 3.4 shows that, even with plagioclase (An=30, estimated by using Drake's (1976) distribution coefficient of Ca

---

Fig. 3.4. Mass transfer (in cation percent) in formation of the anatectic granite, calculated with a modelled restite (Bio50 . Pl50). Anorthite content of the plagioclase in the restite was estimated to be 30% by using Drake's (1976) melt/plagioclase distribution coefficient of Ca. Compare with Fig. 3.3.

between the melt and plagioclase) amounting to 50% in the restite, formation of the anatectic granite leads to mass transfers as above. The only exception to this is for Na, which is slightly gained by the system in this case.

3.4 Discussion and conclusions

The significant gain of K in all the cases discussed above is of particular interest. One critical problem in the transformation from paragneiss to granite is the source of potassium, since potassium feldspar is one of the major mineral phases in granite but is generally absent in paragneiss. A widely accepted explanation is biotite breakdown to K-feldspar during anatexis (Hoscheck 1976; Le Metour 1978; Winkler 1979). However, this work has shown that this mechanism alone is not adequate to account for the observed increase in potassium. Significant amounts of K must be added to the system.

The potassium may have been released from deeper continental crust with a metamorphic fluid, which migrated upwards to the zone of migmatization. At the final stages of anatexis, most of the K may have been fixed in the rocks and the Na may have become relatively enriched in the fluid. This may account for the occurrence of the white pegmatite, which is widely associated with the migmatites in this terrane and has a sodium content almost twice as high as that of the anatectic granite (Tab.3.1).

It has been shown that the observed gradation along the outcrop reflects a largely temperature-controlled migmatization gradient. The low grade migmatization in this region occurred in an almost closed system. Partial melting was the dominant mechanism. As migmatization developed to higher grade, metasomatism began to play an important role. A simple mass-balance calculation considering each major component, with the estimated restite composition based on Winkler's (1979) experiments, has shown that the relatively significant mass transfer involved the gain of K and loss of Ca, Al, Na and Mg during the formation of the diatexite and anatectic granite. This result is generally compatible with that of Olsen (1984). Since the compositions of the paragneiss and granite of this study are quite common, it is suggested that, as a general rule, anatexis alone is inadequate to account for the generation of granite from paragneiss by migmatization. Some mass transfer, particularly the gain of K, seems necessary.

The continuous gradation of migmatization in a relatively short distance accompanied by mass transfer at high grades may be explained by the introduction of a metamorphic fluid which heats and reacts with the host rock (cf. Ferry 1983). There were probably two major agents for heat transport during migmatization: conduction by the rock and advection via the infiltrating fluid. The presence of metamorphic fluid would not only heat the host rock, but also lower its melting point. Olsen (1984) observed that the amount of fluid rather than the

rock's composition determined the extent of melting. The anatectic granite may have been situated close to the channel of the fluid. Its melting would then block the further transportation of the fluid into rocks away from the channel (Arzi 1978). The essentially closed system for the metatexite may indicate that fluid was not involved in its formation, and that the heat was supplied mainly by conduction through the rock. Assuming the difference of partial-melting temperature between the high-grade migmatites and metatexite was completely due to the fluid-heating, and assuming an initial temperature of 800 ^{o}C for the fluid, (anatectic temperatures for diatexite and granite were estimated as 650 ^{o}C - 700 ^{o}C using Ferry and Spear's (1978) garnet-biotite geothermometer, see Appendix-III), a fluid/rock mass ratio of more than 2 may be estimated from heat budget calculations. This ratio is much higher than most of those estimated by Olsen (1984) from modelled fluid compositions for the migmatization in the Colorado Front Range (There was however a great variation of the fluid/rock ratios obtained for each element in Olsen's (1984) study). The discrepency of the ratios in this work and those of Olsen's (1984), and the great variation of the ratios showed in Olsen's own work, may be due to the uncertainty of the compositions of metamorphic fluids (Olsen 1984). On the other hand, the fluid/rock ratio for migmatization in different regions may be quite different, since they are functions of many factors, such as temperature, fluid composition, flow rate, etc., and these factors could vary greatly in various regions.

Table 3.1. Bulk Compositions (in cation percent)

	Biotite -gneiss	Meta- texit	Diatexite neosome	Diatexite biotite	Anatectic granite neosome	Anatectic granite biotite	Anatectic granite restite-B	Pegma- tite
Si	60.34	61.38	69.38	38.43	69.02	36.35	47.29	71.80
Ti	0.35	0.34	0.06	3.35	0.03	2.92	2.27	0.00
Al	17.47	17.14	15.55	18.78	15.85	18.20	17.10	14.54
Fe*	4.05	3.58	0.58	20.55	0.47	26.27	19,96	0.05
Mg	4.26	3.47	0.12	8.22	0.06	5.80	4.30	0.00
Ca	3.17	2.70	0.96	0.00	0.92	0.00	0.46	1.23
Na	7.40	7.86	8.79	0.07	7.27	0.02	1.44	11.38
K	2.91	2.90	4.52	10.60	6.34	10.43	7,33	1.02

Table 3.2. Test of closed-system of migmatization

		Xc(Si)	Xc(Ti)	Xc(Al)	Xc(FE*)	Xc(Mg)	Xc(Ca)	Xc(Na)	Xc(K)
Granite	A	73.4	88.9	31.1	86.1	26.8	344.6	101.8	183.9
	B	60.1	84.3	-22.7	81.6	0.9	589.1	102.2	446.5
Diate- xite	A	70.8	91.2	40.6	82.6	48.9	330.2	84.1	126.5
	B	59.1	85.6	-18.5	82.1	.1.0	542.0	81.1	157.3

Table 3.3. Mass-balance calculation (in cation percent)

Granite

Xo (%)	D(Si)		D(Ti)		D(Al)		D(Fe*)	
	A	B	A	B	A	B	A	B
65	-2.8	1.1	0.7	0.4	-0.8	-1.1	5.5	3.2
75	0.5	3.2	0.4	0.2	-1.0	-1.3	2.9	1.3
85	3.8	5.4	0.1	0.0	-1.3	-1.4	0.3	-0.7
95	7.0	7.6	-0.2	-0.2	-1.5	-1.6	-2.3	-2.6

Xo (%)	D(Mg)		D(Ca)		D(Na)		D(K)	
	A	B	A	B	A	B	A	B
65	-2.2	-2.7	-2.6	-2.4	-2.7	-2.2	4.9	3.8
75	-2.8	-3.2	-2.5	-2.4	-1.9	-1.6	4.5	3.7
85	-3.3	-3.6	-2.4	-2.3	-1.2	-1.0	4.0	3.6
95	-3.9	-4.0	-2.3	-2.3	-0.5	-0.4	3.6	3.5

Diatexite

Xo (%)	D(Si)		D(Ti)		D(Al)		D(Fe*)	
	A	B	A	B	A	B	A	B
65	-1.8	1.3	0.9	0.4	-0.8	-1.4	3.5	3.3
75	1.3	3.5	0.5	0.2	-1.1	-1.5	1.5	1.4
85	4.4	5.7	0.2	0.0	-1.4	-1.7	-0.5	-0.6
95	7.5	7.9	-0.1	-0.2	-1.8	-1.8	-2.5	-2.5

Xo (%)	D(Mg)		D(Ca)		D(Na)		D(K)	
	A	B	A	B	A	B	A	B
65	-1.3	-2.7	-2.5	-2.4	-1.7	-1.2	3.7	2.6
75	-2.1	-3.1	-2.5	-2.3	-0.8	-0.4	3.1	2.3
85	-2.9	-3.5	-2.4	-2.3	0.1	0.3	2.5	2.0
95	-3.7	-3.9	-2.3	-2.2	0.9	1.0	1.9	1.8

Table 3.1. Composition of the rocks were determined by XRF and presented in terms of eight major cations, normalized to 100 precent with total iron calculated as F*. Restite-B is a model restite (Bio70 Pl15 Qz10 Gar5). Composition of biotite gneiss is that of sample 05A. Metatexite is sample 021. Diatexite is sample 026. Anatectic granite is the average of sample 029, 031, 033 and 034.

Table 3.2. Row A shows the results calculated with restite-A (pure biotite). Row B shows the results of using restite-B in the calculations.

Table 3.3. The meaning of A and B is the same as in Table 3.2. The sigh of Di shows the gain or loss of the component by the system (positive for gain and negative for loss).

Chapter 4

SUMMARY AND CONCLUSIONS

Two basaltic sequences and an overlying komatiitic sequence have been recognized in the study area. They may have originated in an Archaean rifting environment. The basalts were probably erupted through continental crust, resulting in the observed abnormal behavior of Rb and K. Chemical variation of the basalts is compatible with a crystal-fractionation-controlled magma evolution. The fractionation process may have been somewhere between fractional crystallization and equilibrium crystallization, with most olivine and some pyroxene crystals removed while most plagioclase and some pyroxene crystals remained in the magmas.

The komatiites, despite their intimate spatial relationship to the basalts and their similar trace element ratios, cannot be the direct parental magmas to the basalts. They may, however, have been derived from the same mantle diapir at different depths. The magmas parental to the basalts may be the products of a lower degree of partial melting at a relatively higher pressure than the komatiites. They may have last equilibrated with the mantle under continental crust at the early stages of rifting. The komatiites may have been produced by increasing degrees of adiabatic partial melting as the diapir rose. They may have last equilibrated with the mantle under newly-formed oceanic crust at the later stages of the rifting.

A rift-propagation from east to west may be responsible for

the observations that 1) the pressure of magma fractionation decreases from east to west in the greenstonne belt and that 2) the proportions of komatiite decrease from Lac Guyer area westwards to the study area and are absent in the western part of the belt.

Although this study suggests the basaltic lavas may have been erupted through continental crust, whether the neighbouring gneissic-granitic terrane represents the very basement on which the basalts were erupted is not clear, mainly due to lack of field evidence. In any event, the gneissic-granitic terrane experienced a major metamorphic-migmatization event, which may have been synchronous with amphibolite-facies metamorphism in the adjacent greenstone belt. A second focus of this research was the problem of migmatization in the gneissic terrane. It is shown that the progressive gradation of migmatization was controlled lagerly by temperature, rather than the bulk compositions of the rocks. The low-grade migmatite was probably formed in an approximately closed system, controlled dominantly by partial melting. As migmatization progressed to higher degrees, metasomatism became important. Mass-balance calculations for the generation of diatexite and anatectic granite show significant mass transfer, particularly the gain of K and loss of Ca, Mg, Al, and Na by the system. Since the compositions of the biotite gneiss and the granite are fairly typical for continental crust in general, it is suggested that , as a general rule, anatexis alone is inadequate for the generation of granite from

paragneiss.

The continuous gradation of migmatization observed in the field and the accompanying mass transfer at high grade may be due to the introduction of a metamorphic fluid from deeper crust. The fluid may have increased the degrees of partial melting by heating the rocks and lowering their melting points, and produced metasomatic exchanges at the same time.

It has been suggested that the greenstone belt may have originated in a continental rifting environment. The rift might also have occurred in back-arc region. This is however diffidult prove since no subduction-associated volcanic rocks have been recognized in the field, although there is a possibility that they may have been reworked and become part of the gneissic-granitic terrane.

Studies of migmatization in the gneissic-granitic terrane have shown the important role played by metamorphic fluids in the generation of migmatites. The widely developed migmatization in the terrane requires a great fluid influx. If we suppose Archaean tectonics is analogous to those today, one possible region for the generation of this type of migmatite terrane is above subduction zone, where a large amount of fluid is produced from degassing and dehydration of the subducting plate. Since we favour a continental rifting model for the evolution of the greenstone belt, the question of what may have coused the high

fluid influx in the neighbouring gneissic-granitic terrane arises. One possible answer to this is that the fluid may have been produced during subsequent crustal thickening consequent on the collapse of whatever oceanic crust was produced in the region. At present, then, it is possible to explain the observed charactristics of the region without involking subduction-related volcanism, or subduction zone, although it is difficult, using modern tectonic analyses, to explain the thermal evolution of the belt without appealing at least to substantial degrees of intercrustal thrusting.

CONTRIBUTIONS TO THE KNOWLEDGE

This study represents a preliminary attempt to understand the tectonic evolution of the La Grande greenstone belt and the migmatization in the neighbouring gneissic-granitic terrane. The following are the major contributions of this study:

1). Two sequences of basalts overlain by a komatiitic sequences have been recognized in the study area.

2). It has been shown that the evolution of the basaltic suites may have been controlled largely by crystal fractionation. The process may be somewhere between fractional crystallization and equilibrium crystallization, with most olivine and probably some pyroxene crystals removed while most plagioclase and some pyroxene crystals remained in the magmas.

3). It has been suggested that the basalts may have erupted through continental crust, resulting in the observed abnormal behaviour of Rb and K. An oceanic crust was probably already formed by the time of komatiite eruption.

4). It has been shown that there is a westward decrease of pressure of magma fractionation in the greenstone belt. This is interpreted to be related to a rift propagated from east to west.

5). It has been shown that the progressive gradation of migmatization in the neighbouring gneissic-granitic terrane was controlled largely by temperature, rather than the bulk composition of the rocks.

6). The metatexite has been shown to have originated in an approximately closed system, controlled dominantly by partial melting.

7). It has been shown that the generation of diatexite and granite from biotite gneiss involved significant mass transfer, particularly the gain of K and loss of Ca, Mg, Na, Al.

8). It has been suggested that the progressive gradation of migmatization with accompanying mass transfer at high grades may be due to the introduction of a metamorphic fluid from deeper crust.

SUGGESTIONS FOR FUTURE WORK

This thesis presents a preliminary study of the evolution of the La Grande River greenstone belt. There are many problems remaining. The following problems are suggested for future work in this region:

1). Relationship of the greenstone belt to the surrounding gneissic-granitic terrane---- More field work and chronological studies may be useful for a better understanding of the relationship of the gneissic-granitic terrane to the greenstone belt, which is of great importance for reconstructing the tectonic history.

2). P-T conditions for the evolution of the igneous rocks in different part of the belt---- Systematic studies of geobarometry and geothermometry in the belt may provide some powerful constraints on tectonic models for the development of the greenstone belt.

3). The nature of metamorphic fluid ---- The temperatures and compositions of the metamorphic fluids may be obtained by fluid-inclusion studies. This is of great importance for a clearer understanding of the role played by metamorphic fluids during the migmatization.

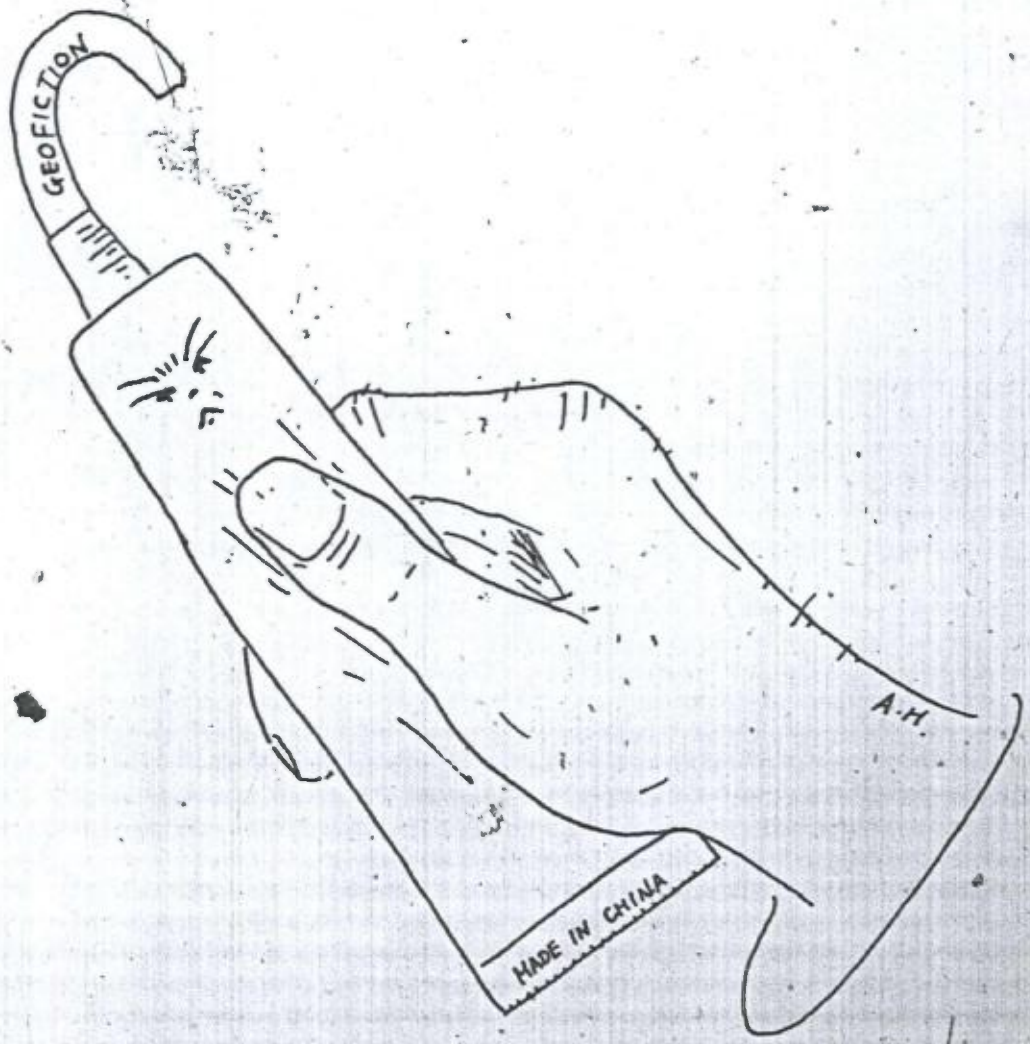
GEOFICTION
A.H.
MADE IN CHINA

REFERENCES

Anderson DH and Gast PW (1965) Uranium-lead zircon ages and lead isotope compositions in two Algloman granites of Northern Minnesota (Abstract). In: Abstracts for 1964: Geol Soc Am, Sp Pap pp. 3-4

Anhaeusser CR, Mason R, Viljoen Mj, Viljioen RP (1969) A re-appeisal of some aspects of Precambrian shield geology. Geol Soc Am Bull 80: 2175-2200

Anhaeusser CR (1973) The evolution of the early Precambrian crust of southern Africa. Philos Trans R Soc London A 273: 359-388

Arndt NT, Nesbitt RW (1982) Geochemistry of Munro Township basalts. IN: Arndt NT, Nesbitt RW (eds) Komatiite. George Allen & Unwin Ltd. London, 309-329

Arth JG, Arndt NT and Naldrett AJ (1977) Genesis of Archean komatiite from Munro Township, Ontario: Trace element evdience. Geology 5: 590-594

Arzi AA (1978) Fusion kinetics, water pressure, water diffusion and electrical conductivity in melting rock, interrelated. J Petrol 19: 153-169

Bedard JH, Francis DM, Hynes AJ and Nadeau S (1984) Fractionation in the feeder system at a Proterozoic rifting margin. Can J Earth Sci 21: 489-499

Bickle MJ, Martin A, Nisbet EG (1975) Basaltic and peridotitic komatiites and stromatolites above a basal unconformity in the Belingwe greenstone belt, Rhodesia. Earth Planet Sci

Lett 27: 155-162

Biggar GM (1983) Crystallization of plagioclase, augite and olivine in synthetic and in tholeiites. Mineral Mag 47: 161-176

Burke K, Dewey JF, and Kidd WSF (1976) Dominance of horizontal movements, arc and microcontinental collisions during the later permobile Regime. In: B.F. Windley (ed) The early history of the Earth, Wiley Intersciences, London, pp 113-129

Bryan WB (1979) Regional variation and petrogenesis of basalt glasses from the FAMOUS area, mid-Atlantic Ridge and Kane Fracture Zone. J Geophys Res 86: 11815-11836

Byerly GB, Wright TL (1978) Origin of major element chemical trends in DSDP leg 37 basalts, Mid-Atlantic Ridge. J Volc Geotherm Res 3: 229-279

Camble RP, Taylor LA (1980) Crystal/liquid partioning in augite: effect of cooling rate. Earth Planet Sci lett 47: 21-33

Cater JL (1970) Mineralogy and chemistry of the Earth's upper mantle based on the partial fusion-partial crystallization model. Bull Geol Soc Am 81: 2022-2034

Cox KG (1980) A model for flood basalt volcanism. J petrol 21: 629-650

Cox KG, Bell JD and Pankhurst RJ (1979) The interpretation of igneous rocks. George Allen & Unwin Ltd, London. pp450.

Doe BR, Lipman PW, Hedge CE and Kurasawa H (1969) Primitive and contaminated basalts from the southern Rochy Mountains, USA. Contr Mineral Petrol. 21: 142-156

Dostal J, Baragar WRA and Dupuy C (1983) Geochemistry and petrogenesis of basaltic rocks from Coppermine River area, Northwest Territories. Can J Earth Sci. 20:684-698

Drake MJ (1976) Plagioclase-melting equilibria. Geochim Cosmochim Acta 40:457-466

Dupuy C, Dostal J (1984) Trace element geochemistry of some continental tholeiites. Earth Planet Sci Lett 67: 61-69

Eade KE (1966) Fort George River and Kiapiskau River (west half) map-area, new Quebec. Geological Survey of Canada, Memoir 339

Elthon D (1984) High-pressure phase equilibria of a high-magnisia basalt and the genesis of primary oceanic basalts. Am Mineral 69: 1-15

Elthon D (1983) Isomolar and isostructural pseudo-liquids phase diagrams for oceanic basalts. Am Mineral 68: 506-511

Ferry JM (1983) Regional metamorphism of the Vassalboro Formation, south-central Maine, USA: a case study of the role of fluid in metamorphic petrogenesis. J Geol Soc London 140: 551-576

Ferry JM, Spear FS (1978) Experimental calibration of the partioning of Fe and Mg between biotite and granet. Contr Mineral Petrol 66: 113-117

Glikson AY (1976). Stratigraphy and evolution of primary and secondary greenstones: significance of data from Shields of the southern hemisphere. In B.F. Windley(ed.), The Early history of the Earth, Wiley, London, 257-277.

Glikson AY (1972) Early Precambrian evidence of a primitive

ocean crust and island nuclei of sodic grannite. Geol Soc Am Bull:83 3325-3344

Hanson GN, Langmuir CH (1978) Modelling of major elements in mantle-melt systems using trace element approaches. Geochim Cosmochim Acta 42: 725-741

Harris NBW (1974) Some migmatite types and their origins, from the Barousse Massif, Central Pyrenees. Geol Mag 111: 319-328

Hart SR, Davis GL (1969) Zircon U-Pb and whole-rock Rb-Sr ages and early crustal development near Rainly Lake, Ontario: Geol Soc Am Bull 80: 595-616

Henderson JB, Easton RM (1977) Archaean supracrusta;-basement rock relationships in the Keskarrah Bay map-area, Slave Structural Province. District of Mackenzie. Geol Surv Can, Pap 77-1A: 217-221

Hoscheck G (1976) Melting relations of biotite+plagioclase+quartz. Neues Jahrb Mineral Mh 2:79-83

Hynes A, Francis D (1982) A transect of the early Proterozoic Cape Smith foldbelt, New Quebec. Tectonopgysics 88: 23-59

Kroner A, Puustinen K and Hickman M (1981) Geochronology of an Archaean tolitic gneiss dome in Northern Finlind and its relation with an unusual overlying volcanic conglomerate and komatiitic greenstone. Contr Mineral Petrol 76: 33-41

Kroner A (1981) Precambrian plate tectonics. In: A Kroner (ed) Precambrian plate tectonics. Elsevier, Amsterdam, pp 57-90

Lambert R St (1981) Earth tectonics and thermal history: review and a hot-spot model for the Archaean. In: Kroner (ed) Precambrian plate tectonics. Elsevier, Amsterdam, pp 453-

Le Mour J (1978) Petrogenesis of migmatites and associated granites in South Brittany. Neues Jahrb Mineral Mh H8:364-376

Leterrier J, Maury RC, Thonon P, Girard D and Marchal M (1982): Clinoroxene composotion as a model of identification of the magmatic affinities of paleo-volcanic series. Earth Planet Sci Lett 59: 139-154

Luth WC, Jahns RH and Tuttle OFF (1964) The granite system at pressure of 4 to 10 kilobars. J Geophys Res 69: 759-733

Maury RC and Bizoaurd H (1974) Melting of acid xenoliths into a basanite: An approch to the possible mechanisms of crustal contamination. Contr Mineral Petrol. 48: 275-286

Mehnert KR (1968) Migmatites and the origin of granites. Elsevier, Amsterdam

Mathez EA (1984) Influence of degassing on oxidation states of basaltic magmas. Nature 310: 371-375

Mills JP (1974) Petrological studies in the Sakami-lake greenstone belt of nothwestern Quebec. Ph.D thesis, University of Kansas, USA

Nathen HD, Van Kirk CK (1978) A model of magmatic crystallization. J Petrol 19: 66-94

Nesbitt RW, Sun SS (1976) Geochemistry of Archean spinifex-textured peridotites and magnisian and low-magnisian tholeiites. Earth Planet Sci Lett 31: 433-453

Nisbet EG (1982) The tectonic setting and petrogenesis of komatiites. In: Arndt NT, Nesbitt RW (eds) Komatiite. George Allen & Unwin Ltd, London. 501-518

Olsen SN (1977) Origin of the Baltimore Gneiss migmatites at Piney Creek, Maryland. Geol Soc Am Bull 88:1089-1101

Olsen SN (1982) Open-and closed- system migmatites in the Front Range, Colorado. Am J Sci 282:1596-1622

Olsen SN (1983) A quantative approach to local mass balance in migmatites. In: Atherton MP,Gribble CD (eds) High grade metamorphism, migmatites and melting. Orpington: Shiva Pub Ltd, pp 201-233

Olsen SN (1984) Mass-balance and mass transfer in migmatites from the Colorado Front Range. Contrb Mineral Petrol 85: 30-44

Pearce JA, Norry MJ (1979) Petrogenetic implications of Ti, Zr, Y, and Nb variations in volcanic rocks. Contr MMineral Petrol 69: 33-47

Ramakrishnan M, Viswanatha MN, Swami Nath J (1976) Basement-cover relationship of Peninsular Gneiss with high-grade schists and greenstone belts of southern Karanataka. J Geol Soc India 17:97-111

Roeder PL, Emslie RF (1970) Olivine-liquid equilibrium. Contr Mineral Petrol 29: 275-289

Rivard B, Francis D (1984) Preliminary models for basalt evolution in the La Grande greenstone-belt. In: Guha J, Chown EH (eds) Chibougonion-stratigraphy and mineralization. CIM special volume 34: 48-56

Skulski T, Hynes A and Francis D (1984). Stratigraphy and lithogeochemical characterization of cyclic colcanism in the LG-3 area, La Grande River greenstone-belt, Quebec. ib. 73-91.

Stolper E, Walker D (1980) Melt density and the average composition of basalts. Contr Mineral Petrol 74: 7-12

St.Seymour K, Francis D and Ludden J (1983) The petrogenesis of the Lac Guyer komatiite and basalts and the nature of the komatiite-komatiitic basalt composition gap. Contr Mineral Petrol 84: 6-14

St.Seymour k (1982) Volcanic petrogenesis in the Lac Guyer greenstone belt, James Bay area, Quebec. Ph.D thesis, McGill University.

St.Seymour, Francis D (1980) Metamorphic olivine in peridotitic komatiite flows, Lac Guyer, Quebec. Can mineral 18: 265-270

Sun SS and Sharaskin AYa (1979) Geochemical characteristics of mid-ocean ridge basalts. Earth Planet Sci Lett 44: 119-138

Tarney J, Dalziel IWD,and De Wit MJ (1976) Marginal basin "Rocas Verdes" complex from S.Chile: a model for Archaean greenstone belt formation.In: B.F.Windley (ed) The Earth history of the Earth. Wiley, London pp 131-146

Tilton GR, Steiger RH (1969) Mineral ages and isotopic composition of primary lead at Manitouwadge, Ontario: J Geophys Res 74: 2118-2132

Van Schmus WR, Hayes JM (1974) Chemical and petrographic correlations amoumg carbonaceous chondrites. Geochim Cosmochim Acta 38: 47-64

Viljoen MJ, Voljoen RP (1969) The geology and geochemistry of the lower ultromafic unit of the Quverwacht Group and a proposed new class of ignious rocks. Spec Pulb Geol Soc S Africa 2: pp55.

Viljoen MJ, Viljoen RP (1970) Archean volcanicity and continental

evolution in Barberton region, Transval. In: PN Clifford and I Gass (eds) African magmatism. Oliver & Boyd, Edinburgh, pp 27-49

Wanke H, Baddenhausen H, Palme H and Spettel B (1974) On the chemistry of the allende inclusions and their origin as high-temperature condensates. Earth Planet Sci Lett 23: 1-13

Watson EB (1982) Basalt contamination by continental crust: some experiments and models. Contr Mineral Petrol. 80: 73-87

Whitney JA, Stormer JC (1977) The distribution of NaAlSi308 between co-existing microcline and plagioclase and its effect on geothermotric calculation. Am Mineral 62:687-691

Windley BF (1977) The evolving continents. John Wiley & Sons, New York, pp.63

Winkler HGF (1979) Petrogenesis of metamorphic rocks. 5th ed, Spring-Verlag, New York, pp 283-339

Yardley BWD (1978) Genesis of Skagit Gneiss migmatites, Washington, and the distinction between possible mechanisms of migmatization. Geol Soc Am Bull 89:941-951

APPENDIX I. ANALYTICAL PROCEDURES

X-Ray Fluorescence Analyses

All whole rock major and trace element concentrations were determined by X-Ray Fluorescence techniques, using a Philips PW-1400 spectrometer with a 100 KV generator in the Department of Geological Sciences at McGill University. Major element (plus Cr and Ni) standardization was acheived by comparing net peak counts-per-second corrected for mass absorption with a calibration line derived from 18 international reference materials. The precision is 0.2% (absolute).

Trace elements were determined from peak- and five background-counts per second. The background data were used to calculate a best-fit background curve of the form :

$$C = a + b \exp(t) + c \exp(2t) + d \exp(3t) + e \exp(4t)$$

where C is the background and t is the value of 2 . Since some of the background positions are subject to interference, empirical corrections (based on diluted "spike" tests) were applied to the backgrounds, using the net peaks for elements at lower 2 positions. Several successive background curves were calculated, incorporating net peaks of elements with progressively lower 2 positions. Empirical interference corrections were also applied to the peaks. Net peaks were corrected for mass-absorption using mass absorption coefficients

from the major-element analyses. Standardization of the trace element was acheived by comparing with calibration lines from a set of diluted spikes. This calibration was preferred over that based on international standards, because there is considerable inhomogeneity in many of the international standards at the levels of concern in this study. Nevertheless, variations between the spike-derived calibrations and those using an international standard data-set are less than 5 % in all cases.

Electron-probe Analyses

Mineral (feldspar, garnet and biotite) compositions were obtained using the CAMEBAX electron microprobe (Model MB1) in the Department of Geological Sciences at McGill University. The results were corrected for mass absorption with the ZAF correction program (Cameca software). For feldspar and biotite, the following standards from the standard block supplied by Cameca was used: orthoclase for Si, Al, K; MnTiO3 for Ti and Mn; andradite for Fe and Ca and albite for Na and MgO for Mg. For garnet analyses the standards used were: Olivine for Mg and Fe; spessartine for Si and Al; MnTiO3 for Ti and Mn; andradite for Ca. The analyses were performed by a wave length dispersive method with four spectrometers. The working voltage was 15 KV and the intensity for the beam was 8 ua. The counting time was 20 seconds. Precision for element concentrations is 1 %. For microcline, defocused beam (20 microns) was used in an attempt to obtain more representative values.

≠ V4 mais plutôt V I4

APPENDIX II. BULK COMPOSITIONS OF THE ROCKS

(The oxdites are in weight percent. The trace elements are in ppm)

Table II-1 Composition of the komatiite

Idem à la page 34

Sample#	83132	83232	83432	83039	83040	83052	83070
SiO2	42,87	43.15	47.18	44.34	44.42	44.73	54.78
TiO2	0.26	0.18	0.28	0.49	0.32	0.46	0.13
Al2O3	2.77	2.75	3.63	6.76	6.77	6.82	1.92
Fe2O3	12.86	13.35	17.22	16.43	14.36	14.48	8.68
MgO	39.19	40.64	31.90	27.37	28.49	25.83	25.28
MnO	0.22	0.18	0.27	0.19	0.20	0.23	0.17
CaO	2.32	0.58	0.26	5.21	5.86	5.21	10.81
Na2O	0.04	0.06	0.13	0.03	0.06	0.08	0.01
K2O	0.02	0.00	0.01	0.01	0.01	0.01	0.01
P2O5	0.01	0.00	0.00	0.04	0.04	0.03	0.01
Total	100.67	100.98	100.98	100.92	100.55	97.93	101.82
Cr	573	449	564	313	24	294	102
Ni	224	155	127	9	91	90	49
NB	0	0	0	0	0	0	0
ZR	10	7	8	29	16	23	4
Y	4	3	2	13	9	11	9
SR	8	7	3	8	31	26	10
RB	4	2	2	2	1	2	0
Al_2O_3/TiO_2	10,65	15,28	12,96	13,80	21,16	14,83	14,77

V

Table II-1 (continued)

Composition of the komatiite

Sample#	83071	83073	83181
SiO2	43.91	42.02	50.02
TiO2	0.40	0.28	0.56
Al2O3	4.50	3.39	8.67
Fe2O3	14.89	14.43	9.57
MgO	32.10	37.61	22.24
MnO	0.22	0.17	0.17
CaO	4.92	1.95	8.24
Na2O	0.04	0.05	0.50
K2O	0.01	0.01	0.12
P2O5	0.03	0.03	0.30
Total	101.08	100.05	100.42
Cr	328	602	141
Ni	132	200	86
NB	0	0	0
ZR	17	10	65
Y	7	4	12
SR	11	5	30
RB	0	1	4
	11.25	12.11	15.48

moyenne: 14.29

Table II-2 Composition of the basalt

Sample#	83016	83117	83030	83131	83034	83037	83146	83062	83065
SiO2	50.88	48.49	50.75	51.40	48.38	48.35	48.84	49.14	49.48
TiO2	1.25	0.83	0.82	1.02	0.94	0.50	0.67	0.70	0.95
Al2O3	14.41	16.92	17.70	14.65	15.18	14.17	16.27	16.95	14.58
Fe2O3	14.30	12.89	12.20	12.31	15.43	11.87	12.02	11.82	14.32
MgO	5.47	6.74	7.06	8.15	7.93	13.41	9.19	9,27	7.29
MnO	0.37	0.21	0.19	0.20	0.23	0.17	0.20	0.18	0.22
CaO	11.00	11.30	9.35	10.39	10.59	10.01	10.94	8.97	11.82
Na2O	2.85	2.58	2.93	2.57	2.14	1.31	2.48	2.21	1.38
K2O	0.59	0.59	0.75	0.54	0.24	0.79	0.25	1.58	0.61
P2O5	0.08	0.05	0.05	0.46	0.04	0.03	0.03	0.05	0.06
Total	101.20	100.60	101.80	101.69	101.10	100.63	100.90	100.88	100.71
Cr	17	24	18	23	16	83	47	23	12
Ni	6	8	6	7	8	28	11	16	6
NB	4	0	0	0	0	0	0	0	0
ZR	59	40	37	43	40	21	29	33	46
Y	25	20	18	17	20	12	15	15	21
SR	127	247	139	134	143	68	151	233	159
Rb	37	28	30	23	11	51	7	87	27

Table II-2 (continued). Composition of the basalt

Sample#	83066	83067	83068	83072	83079	83080	83082	83386	38
SiO2	51.15	52.49	49.57	50.21	50.46	49.29	50.10	50.72	48.47
TiO2	1.17	1.84	0.43	0.81	1.15	0.96	0.72	0.79	0.82
Al2O3	14.83	12.19	16.91	15.41	15.79	15.16	15.34	15.13	15.27
Fe2O3	13.97	20.08	9.44	10.83	14.11	14.71	11.64	11.23	13.08
MgO	6.34	3.93	9.11	7.57	5.54	8.57	9.12	9.13	9.50
MnO	0.24	0.35	0.15	0.16	0.20	0.21	0.18	0.18	0.21
CaO	11.16	7.03	12.47	12.56	11.93	9.85	12.14	10.98	10.48
Na2O	1.62	2.60	1.24	2.79	1.69	2.25	1.83	2.84	2.32
K2O	0.24	0.14	1.44	0.65	0.16	0.20	0.19	0.18	0.45
P2O5	0.07	0.10	0.02	0.05	0.07	0.06	0.03	0.05	0.05
Total	100.79	101.56	102.36	102.34	101.44	101.64	101.86	101.63	101.46
Cr	11	5	720	7	14	20	370	41	34
Ni	6	1	90	5	4	11	90	12	10
NB	0	0	0	0	0	0	0	0	0
ZR	55	78	17	37	51	46	37	38	39
Y	24	37	10	14	24	20	16	18	18
SR	92	19	106	231	131	99	156	113	161
RB	4	4	74	27	2	1	4	0	22

Table II-3 Composition of the gneissic rocks

Sample#	05A	14D	16B	17	18	59	83109	83110	83119
SiO2	64.53	66.60	67.01	64.35	62.21	64.33	61.18	64.43	69.96
TiO2	0.59	0.53	0.49	0.51	0.52	0.50	0.61	0.54	0.23
Al2O3	15.98	15.06	15.12	15.57	15.97	5.45	17.79	14.93	15.60
Fe2O3	6.27	6.21	4.63	5.33	5.67	5.45	7.35	6.38	3.06
MgO	3.66	3.21	1.72	3.19	3.29	3.17	4.17	3.04	1.46
MnO	0.05	0.08	0.06	0.08	0.07	0.07	0.06	0.08	0.09
CaO	3.00	2.38	3.33	3.85	3.55	3.31	2.60	4.14	2.87
Na2O	2.80	3.88	5.41	4.52	4.24	4.30	4.01	4.29	5.14
K2O	2.85	2.69	2.02	2.66	3.01	2.79	2.95	1.97	1.72
P2O5	0.12	0.12	0.18	0.24	0.27	0.24	0.14	0.13	0.14
Total	99.85	100.76	99.97	100.30	98.80	89.61	100.86	99.93	100.27
NB	2	2	2	3	4	4	5		
ZR	117	105	134	127	132	133	108		
Y	14	11	14	12	15	14	26		
SR	565	287	731	1070	1529	1368	239		
RB	136	163	57	83	127	153	111		

Table II-3-2 Composition of the migmatite and granite

Sample#	21	24	26	28	29	31	132	33	34
SiO2	65.83	75.23	74.79	73.92	74.56	74.62	73.87	74.41	73.26
TiO2	0.58	0.03	0.08	0.02	0.05	0.01	0.16	0.05	0.07
Al2O3	15.82	13.76	14.22	14.60	14.46	14.35	13.83	14.25	14.61
Fe2O3	6.26	0.45	0.83	0.48	0.56	0.52	1.64	0.82	0.95
MgO	3.14	0.04	0.09	0.00	0.03	0.01	0.19	0.08	0.11
MnO	0.05	0.01	0.03	0.01	0.01	0.01	0.02	0.01	0.01
CaO	2.52	0.38	0.97	0.67	1.04	0.80	0.86	1.08	1.02
Na2O	3.64	3.26	4.89	3.65	4.48	4.22	3.39	3.83	3.96
K2O	2.28	6.64	3.82	6.56	4.31	5.23	5.59	5.21	5.40
P2O5	0.11	0.02	0.02	0.12	0.02	0.02	0.06	0.02	0.04
Total	100.23	99.82	99.74	100.03	99.52	99.79	99.61	99.76	99.43
NB	3	0		0	0	0	0		0
ZR	106	17		25	47	38	172		106
Y	10	26		6	7	27	7		6
SR	528	93		416	134	51	164		226
RB	84	287		271	163	180	188		125

Table II-3-2 (continued)

Composition of the migmatite and granite

Sample#	48	83120	83123	83124	83126	83128	14A	14B
SiO2	77.11	74.12	73.59	72.71	72.94	73.28	73.21	72.20
TiO2	0.00	0.05	0.09	0.10	0.14	0.14	0.00	0.23
Al2O3	13.25	14.77	14.58	14.74	14.99	14.80	15.27	15.68
Fe2O3	0.07	0.71	1.04	1.25	1.47	1.38	0.19	1.97
MgO	0.00	0.07	0.15	0.21	0.27	0.28	0.00	0.71
MnO	0.01	0.01	0.02	0.02	0.02	0.05	0.00	0.02
CaO	1.23	1.19	1.01	0.96	1.14	1.15	0.84	2.90
Na2O	6.28	4.37	4.03	4.05	4.38	3.92	3.69	5.28
K2O	0.86	4.71	5.19	5.44	4.59	5.08	6.50	0.80
P2O5	0.02	0.02	0.04	0.04	0.03	0.04	0.02	0.06
Total	98.83	100.02	99.74	99.52	99.97	100.12	99.72	99.85
NB		0	2	2	2	0	0	0
ZR		70	97	134	132	153	117	205
Y		7	6	14	11	14	5	11
SR		176	158	148	135	215	170	236
RB		153	180	198	149	116	117	110

APPENDIX III. GEOTHERMOMETRY

Table III-1. Garnet-biotite geothermometry*

Sample#		X(Fe)	X(Mg)	KD	T(°C)
20	Bio	45.3	54.6		
	Gar (rim)	81.3	18.6	0.16	542
	Gar (core)	77.9	22.1	0.20	615
21	Bio	42.9	57.1		
	Gar (rim)	80.4	19.6	0.18	589
	Gar (core)	78.6	21.4	0.20	629
128	Bio	70.4	29.6		
	Gar	92.3	7.7	0.20	618

* Temperature calculated using Ferry and Spear's (1978) garnet-biotite geothermometer. KD = (Mg/Fe)Gar/(Mg/Fe)Bio.

Table III-2. Feldspar-thermometry*

Sample#	X(AF)	X(Ab)	T (°C)
22	3.4	84.7	325
24	3.0	83.1	327
26	4.0	86.4	350
29	3.6	84.6	341
	7.1	98.0	389
31	4.5	86.5	369
	18.8	86.2	555

* Temperature calculated using Whitney and Stormer's (1978) feldspar-geothermometer. X(AF) and X(PL) are the mole fractions of albite in alkali feldspar and plagioclase, respectively.

APPENDIX IV. MINERAL COMPOSITIONS

Table IV-1. Composition of biotite

Sample#	SiO2	TiO2	Al2O3	MgO	FeO	MnO	CaO	Na2O	K2O	Total
109	36.76	1.63	18.96	12.08	17.03	0.11	0.00	0.28	9.75	96.59
05A	37.35	2.04	18.11	12.59	17.21	0.12	0.00	0.32	8.99	96.71
20	36.87	1.85	19.96	11.63	17.43	0.11	0.00	0.34	9.21	97.41
21	36.24	1.81	18.99	12.85	16.50	0.05	0.00	0.23	9.13	95.84
26	36.53	3.18	17.85	7.79	19.54	0.94	0.00	0.07	10.08	95.99
27	35.92	3.60	16.70	6.44	23.48	0.62	0.00	0.06	10.18	96.98
32A	34.48	2.77	17.26	5.50	24.92	0.29	0.00	0.03	9.89	95.13
120	35.37	2.53	17.68	7.22	22.27	0.57	0.02	0.08	9.89	95.63

Table IV-2. Composition of garnet

Sample#	SiO2	TiO2	Al2O3	MgO	FeO	MnO	CaO	Total
20(rim)	37.40	0.06	21.01	4.20	31.29	4.71	1.07	99.79
20(core)	37.48	0.00	21.16	4.87	30.78	4.56	1.00	99.85
21(rim)	37.63	0.02	21.15	4.50	30.90	3.92	1.37	99.49
21(core)	39.03	0.00	21.97	4.95	32.44	4.12	1.42	100.04
128	36.76	0.00	20.79	1.31	28.22	11.01	1.62	99.72

Table IV-3. Composition of feldspar

A. Plagioclase

Sample#	SiO2	Al2O3	MgO	FeO	MnO	CaO	Na2O	K2O	Total
05A	58.53	26.16	0.02	0.03	0.01	7.31	6.80	0.03	99.08
20	62.02	23.61	0.00	0.00	0.00	5.34	8.03	0.09	99.09
21	61.39	24.00	0.00	0.03	0.03	5.56	8.37	0.09	99.47
22	65.10	22.31	0.03	0.03	0.04	2.85	9.23	0.15	99.92
24	66.12	21.93	0.02	0.05	0.00	2.94	8.90	0.15	100.10
26	67.02	21.58	0.00	0.06	0.00	2.42	9.24	0.18	100.63
29	69.12	20.63	0.02	0.04	0.01	0.30	10.61	0.09	100.81
32A	65.29	21.93	0.00	0.04	0.02	2.33	9.21	0.12	99.10
128	65.08	21.95	0.02	0.07	0.00	3.53	8.98	0.13	99.76

B. Alkali feldspar

Sample#	SiO2	Al2O3	MgO	FeO	MnO	Na2O	K2O	Total
22	64.10	18.91	0.00	0.06	0.01	0.40	16.89	100.53
24	64.63	18.43	0.02	0.00	0.00	0.34	16.96	100.38
26	65.19	18.15	0.01	0.01	0.01	0.46	16.96	100.80
29	64.24	18.99	0.03	0.06	0.05	0.42	17.08	100.87
31	65.20	18.38	0.04	0.01	0.00	0.88	16.19	100.70
128	64.51	18.46	0.00	0.07	0.05	0.42	16.60	100.11